HIGH PRECISION IDENTIFICATION OF AN OBJECT: OPTIMALITY-CONDITIONS-BASED CONCEPT OF IMAGING[*]

VICTOR A. KOVTUNENKO[†] AND KARL KUNISCH[‡]

Abstract. A class of inverse problems for the identification of an unknown geometric object from given measurements is considered. A concept for object imaging based on optimality conditions and level sets is introduced which provides high resolution properties of the identification problem and stability to discretization and noise errors. As a specific case, the identification of the center of a test object of arbitrary shape and unknown boundary conditions from d boundary measurements in d spatial dimensions in the context of the Helmholtz equation is described in detail. For analysis and numerical realization, methods from topology optimization, generalized singular perturbations endowed with variational techniques, and a Petrov–Galerkin enrichment within generalized FEM are used.

Key words. inverse problem, object identification, topology optimization, singular perturbation, variational methods, optimality condition, level sets

AMS subject classifications. 35R30, 35Q93, 49Q10, 65K10

DOI. 10.1137/13091172X

1. Introduction. The problem of identification of a geometric object (the defect, obstacle, scatterer) and reconstruction of its geometric and physical parameters from given measurements has numerous applications in the engineering and biomedical sciences, in the context of nondestructive testing with acoustic, elastic, and electromagnetic waves. From a mathematical point of view, object identification is an inverse problem, which belongs to the field of shape and topology optimization, system identification, and parameter estimation. For general approaches to inverse and ill-posed problems we refer, e.g., to [26, 37, 40, 52, 54], and the references given there.

Shape optimization approaches to the identification problem were developed in, e.g., [4, 5, 6, 19, 23, 41, 45]. Recently, the concept of topological derivatives was adapted to this field in [7, 11, 16, 32, 51]. Methods of topological analysis are inherently connected with singular perturbations; see [34, 48, 49]. In fact, for the task of identification, a trial geometric object put in a test domain is examined by reducing the trial object from a finite to an infinitesimal one, thus changing the topology of the test domain.

Classic methods, however, are frequently restricted to simple shapes of the test object given in parametrized form and to prescribed boundary conditions. Commonly, either Dirichlet (the sound soft) or Neumann (the sound hard) conditions are assumed a priori. Evidently, this assumption is inconsistent from a physical point of view. In [11] transmission problems are considered. Moreover, in [12, 14] high resolved imaging functionals are derived. Motivated by physical consistency we aim at a priori unknown geometric and scattering properties of a test object.

[†]KF-University of Graz and Graz University of Technology, 8010 Graz, Austria; and Lavrent'ev Institute of Hydrodynamics, 630090 Novosibirsk, Russia (victor.kovtunenko@uni-graz.at).

[‡]Institute for Mathematics and Scientific Computing, KF-University of Graz, 8010 Graz, Austria (karl.kunisch@uni-graz.at).

For identifying arbitrary geometric and physical variables, we utilize asymptotic methods of singular perturbation theory and combine them with variational techniques. Our generalized variational approach to singular perturbations allows us to treat arbitrary shapes as well as unknown boundary conditions of the test object in a unified way. In fact, we use a Robin type (the surface impedance) condition with unknown parameter; see [25, 53]. To be of broad scope we allow it to be spatially dependent. From a mathematical point of view, the impedance parameter is useful for the purpose of regularization as described in [27]. Moreover, as we will show, Robin conditions will play a crucial role for obtaining optimality conditions which are suitable for high resolution reconstruction.

For reconstruction of an object either iterative or noniterative approaches can be used. In the former, a geometric test object is reconstructed iteratively in the descent direction of an objective function. This method is used often for computing, and it is incorporated usually in the level set framework as described in [2, 18, 20, 36]. However, iterative methods have large computational costs.

Within noniterative approaches, a test object is to be reconstructed directly from a single (one shot) or a multiple measurement. The theoretical background is that a so-called far field pattern is uniquely determined by the object; see [1, 29]. To reconstruct the test object from the far field asymptotic pattern, there are well-known sampling and probe techniques such as linear sampling (in particular, factorization), orthogonal sampling, singular and point sources, and other relevant methods; see [21, 26, 35, 40]. The sampling technique in bounded domains results in asymptotic factorization of the Neumann-to-Dirichlet operator as described in [8]. The inverse methods use tests under a single measurement by one harmonic wave (see [47, 50]), as well as multiple measurements by several incident waves either with one or several frequencies (see [31, 46]). In engineering practice, there are well-established multiple signal classification (MUSIC)-type algorithms, which utilize asymptotic approximations obtained from multiple sources; see [9, 10, 13, 22, 28]. In [9, 10] the effect of noise on the imaging functional is considered.

In spite of the evident benefit of the direct approaches, the main difficulty concerns instability and low resolution of imaging of the test object. In this respect, many refined studies for imaging with noisy data were carried out in [7].

To improve stability and resolution properties of object imaging we suggest in the present paper a novel direct approach based on optimality conditions and level sets. Our approach is an optimization theoretic one. We utilize the necessary optimality conditions for finding extrema of an objective function with respect to trial geometric variables (which admit, generally, multiple extrema). Henceforth we can reconstruct the test object directly from the extremal values which associate an imaging function with respect to input data and measured output data. For geometric realization of the imaging function deduced from proper measurements, we relate the respective (multiple) images to level set functions. Hence, the test object can be imaged precisely from its zero sets. As result we obtain a robust and highly accurate numerical method for object identification.

In section 2 we describe the general framework of the procedure that we propose for high precision object identification. The proposed concept is applied to the specific problem of center identification of obstacles in the Helmholtz equation in section 3. The practical strength is demonstrated by means of numerical tests.

2. The optimality-conditions-based concept of object imaging. We start with a geometric description.

Let $\Omega \subset \mathbb{R}^d$, $d \in \mathbb{N}$, be a test domain, which can be bounded or unbounded. Although the degenerate case of $d = 0$ implying a discrete set Ω of points can be accounted for, we henceforth refer to continuous geometries Ω in $\mathbb{R}^d$, $d = 1, 2, 3$. Let a test object be given by the compact set $\omega_{\varepsilon^\star}^\star(x^\star) = \{x \in \mathbb{R}^d : \frac{x - x^\star}{\varepsilon^\star} \in \omega^\star\} \subset \Omega$ which is parametrized by an admissible triple of the shape $\omega^\star \in \Theta_\omega$, the center $x^\star \in \Theta_x$, and the size $\varepsilon^\star \in \Theta_\varepsilon$. The shape $\omega^\star$ is called admissible if is a compact subset in $\mathbb{R}^d$ which is contained in the minimum enclosing ball $B_1(0)$ of radius one centered at the origin 0. Thus, the admissible shapes are invariant to translations and isotropic scaling. The set of admissible geometries $\Theta = (\Theta_\omega, \Theta_\varepsilon, \Theta_x) \subset \mathbb{R}^d \times \mathbb{R}_+ \times \mathbb{R}^d$ consists of those for which $\omega_{\varepsilon^\star}^\star(x^\star) \subset \Omega$.

In the ideal case, the task of identification consists in determining the complete set of geometric parameters $(\omega^\star, \varepsilon^\star, x^\star)$, which is unrealizable practically except in special cases of simple predetermined shapes. In practice, a reasonable goal is to identify a particular geometry $\chi^\star$ deduced from $(\omega^\star, \varepsilon^\star, x^\star)$. For example, the center $x^\star$, the equivalent ball $B_{\varepsilon^\star}(x^\star)$ of radius of $\varepsilon^\star$ centered at $x^\star$, an equivalent ellipse (see [11, 42]) or superellipses, and the like. Since the latter geometric objects are predetermined by the test object, we refer to $\omega_{\varepsilon^\star}^\star(x^\star)$ as the parent object, and to $\chi^\star$ as its child object. In particular, $\chi^\star = \omega_{\varepsilon^\star}^\star(x^\star)$ and $\chi^\star = \partial \omega_{\varepsilon^\star}^\star(x^\star)$ are allowed. In the example configurations we focus on the case $\chi^\star = x^\star$ implying the task of identifying the center of the object. In comparison with $\omega_{\varepsilon^\star}^\star(x^\star)$, the child object $\chi^\star \subset \Omega$ is assumed to be a "regular" geometric set of Hausdorff dimension $d - m$, where the index $0 \leq m \leq d$ specifies the codimension of $\chi^\star$ in $\mathbb{R}^d$. Thus, $\chi^\star$ can be a subdomain of Ω for $m = 0$, a point for $m = d$, and a manifold for $0 < m < d$.

With the above geometric notation we are now in position to formulate the notion of imaging of $\chi^\star$ on the basis of input and measured output data.

Let D^{input} denote fixed input data (inputs) of the underlying problem, in particular, D^{input} may include the test domain Ω itself. A measurement (which can be done in the test domain, at its boundary, in points of receivers, and alike) provides output data (outputs) $D^{\text{output}} := \mathcal{M}(D^{\text{input}}, \omega_{\varepsilon^\star}^\star(x^\star))$ measured with respect to the inputs and the test object $\omega_{\varepsilon^\star}^\star(x^\star)$. Because the test object is generally unknown a priori, the measurement function $\mathcal{M}$ is not available directly, but only the input and output data are at hand. Since the class of physical and topological properties of test objects $\omega_{\varepsilon^\star}^\star(x^\star)$ is predetermined, the combined data $(D^{\text{input}}, D^{\text{output}}) := D$ serve to image some deduced characteristics of the mapping $\mathcal{M} : (D^{\text{input}}, \omega_{\varepsilon^\star}^\star(x^\star)) \mapsto D^{\text{output}}$. Below we get an abstract concept of the deduced imaging of a child test object $\chi^\star$ of $\omega_{\varepsilon^\star}^\star(x^\star)$.

We consider a set of data $\mathcal{D} = \{D\}$, where $D = (D^{\text{input}}, D^{\text{output}})$ consists of the inputs and outputs. We assume that for every datum $D \in \mathcal{D}$ its image $I = \mathcal{I}(D)$ is known by means of the mapping

$$(2.1) \qquad \mathcal{I} : \ D \mapsto I, \ \mathcal{D} \mapsto C(\Omega),$$

with a scalar continuous function $I(x)$, $x \in \mathbb{R}^d$, defined on Ω. We note that neither injectivity nor surjectivity is assumed for $\mathcal{I}$. We use $\mathcal{I}$ in (2.1) to image (reconstruct) the object in Ω by inversion of $\mathcal{M}$ at a specific D. In this respect we get the following definition.

DEFINITION 2.1. *The family of images $\mathcal{I} = \{I\}$ in (2.1) is called the imaging or identification function.*

We will derive the imaging function $\mathcal{I}$ from optimality conditions for specific objective functionals. Usually, optimality conditions of first order have the form of

Euler–Lagrange equations $I(x) = 0$ for $x \in \chi^\star$, which can be expressed equivalently with the help of the zero set $\{x : I(x) = 0\} \supset \chi^\star$. In this case, we declare feasibility of I resulting in the next definition.

DEFINITION 2.2. *An image $I = \mathcal{I}(D)$ in (2.1) is called feasible (with respect to $\chi^\star$), if*

$$\chi^\star \subset Z(I), \tag{2.2}$$

where $Z(I)$ denotes the zero set of I, i.e.,

$$Z(I) := \{x \in \Omega : \ I(x) = 0\} \subset \Omega. \tag{2.3}$$

It is clear that fulfillment of (2.2) does not guarantee uniqueness of $\chi^\star$. From a geometrical viewpoint, a set of points $\chi^\star$ in $\mathbb{R}^d$ can be described uniquely from at least one and at most d implicit surfaces. We arrive at the following notion of identifiability of test objects.

DEFINITION 2.3. *A parent test object $\omega_{\varepsilon^\star}^\star(x^\star)$ is called identifiable by the imaging function $\mathcal{I}$ with respect to its child object $\chi^\star$ of codimension $0 \le m \le d$ in $\mathbb{R}^d$, if there exist $1 \le L \le d$ pairwise different nontrivial feasible images such that*

$$\chi^\star = \bigcap_{i=1}^{L} Z(I_i), \quad I_i = \mathcal{I}(D_i), \quad i = 1, \dots, L. \tag{2.4}$$

Those I_i in (2.4) are called proper images (with respect to $\chi^\star$).

By trivial images here we mean those $I_i(x) \equiv 0$ which result in $Z(I_i) = \Omega$.

If $L = 1$, then Definition 2.3 corresponds to the situation where a single image $I_1 = \mathcal{I}(D_1)$ is sufficient to identify the test object as $\chi^\star = Z(I_1)$. If $L > 1$, then (2.4) needs multiple images I_i deduced from multiple measurements of the parent test object as $i = 1, \dots, L$. For example, for identifying the object center $x^\star$ as a spatial point in 2 or 3 dimensions, the subsequent considerations show that exactly $L = d$ images are needed.

Definition 2.3 is related inherently to the geometric concept of level sets and implicit surfaces. Indeed, under reasonable regularity assumptions, a manifold $\chi^\star$ of codimension $2 \le m \le d$ can be expressed, on the one hand, as the intersection $\chi^\star = \cap_{i=1}^m Z(\rho_i)$ of zero sets of m signed distance functions ρ_i due to [30]. This issue concerns also cracks as open manifolds which appear in high codimension due to the presence of crack tips; see [38, 39]. On the other hand, a measurable geometric set $\chi^\star$ admits the representation as $\chi^\star = Z(\rho_0)$ with the help of a scalar-valued nonnegative distance function $\rho_0 \ge 0$ within the implicit surface context as described in [3, 43, 44]. In this sense, proper images are associated with level set functions.

It is difficult to get any sufficient criterion which would determine a priori an image as proper or not. Therefore, it may be helpful to relax (2.4) with the necessary criterion of identifiability

$$\chi^\star \subset \bigcap_{i=1}^{L} Z(I_i), \quad I_i = \mathcal{I}(D_i), \ i = 1, \dots, L, \tag{2.5}$$

which is suitable for $1 \le L \le d$ feasible images I_i.

For illustration of our concept we present the numerical result for identification of a test point $x^\star =: \chi^\star$, which has Hausdorff dimension zero, hence, the
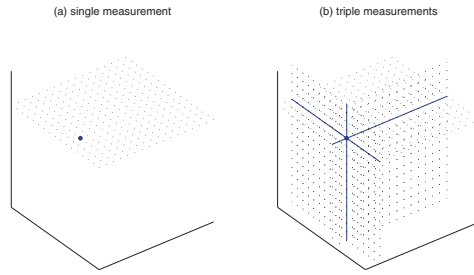
FIG. 1. *Identification of the spatial point from single and triple images.*

codimension $m = 3$ in 3 dimensions in the unit cube Ω. In the example configuration, the sound soft test point is illuminated with plane waves of the form $g(x) = e^{ik(\cos\theta_1 \sin\theta_2 x_1 + \sin\theta_1 \sin\theta_2 x_2 + \cos\theta_2 x_3)}$, where $k \in \mathbb{R}$ stands for the wave number, and $\theta = (\theta_1, \theta_2) \in (-\pi, \pi] \times [0, \pi]$ implies the angle of incidence. Here the inputs yield $D^{\text{input}} = \{\Omega, k, g\}$, and the output D^{output} results from the respective field scattered by the test obstacle $\chi^\star = x^\star$ which is measured at the boundary $\partial\Omega$. After discretization of the underlying Helmholtz problem on the computational domain $\Omega_h = \Omega$ endowed with the uniform polyhedral mesh G_h of size h, we get the discretized data $D^h = (D^{(h,\text{input})}, D^{(h,\text{output})})$ and compute its discretized image $I^h = \mathcal{I}^h(D^h)$. The construction of the imaging function will be described in detail in section 3.

The imaging under a single measurement with the incident angle $\theta^{(1)} = (0, 0)$, the discrete zero set $Z^h(I_1^h)$ of the respective image $I_1^h = \mathcal{I}^h(D_1^h)$, is represented by a number of dots depicted in Figure 1(a). The dots lie exactly on the horizontal plane $Z(I_1^h)$ in the continuous space. The test obstacle $\chi^\star$, marked by the solid blue point, lives within $Z^h(I_1^h)$. Thus, $\chi^\star \subset Z^h(I_1^h) \subset Z(I_1^h)$ and I_1^h is a feasible image. Similarly, for the incident angles $\theta^{(2)} = (\frac{\pi}{2}, 0)$ and $\theta^{(3)} = (\frac{\pi}{2}, \frac{\pi}{2})$ we obtain feasible images given by $I_2^h = \mathcal{I}^h(D_2^h)$ and $I_3^h = \mathcal{I}^h(D_3^h)$. Then the test point is determined by (2.4) as the unique point of intersection of the zero sets $\{Z^h(I_i^h)\}_{i=1}^3$, which lie on three pairwise perpendicular planes $\{Z(I_i^h)\}_{i=1}^3$ as depicted in Figure 1(b). Therefore, these three images are proper. The identification according to (2.4) holds true from the measurements under three different incident angles. This example justifies Definition 2.3 with the number of images $L = m = d = 3$.

In the presented example, we obtain the identification result which is independent of the mesh size for all fine as well as coarse meshes to be reported later. The example configuration is confined to the ideal situation when the test point coincides with the mesh nodes. Otherwise, we report the discretization error of the order $\mathrm{O}(h^4)$, which is negligible within finite elements. To the best of our knowledge, such precise results were not available in the literature. In this respect, the choice of imaging functions is crucial here. In fact, the reason for our high precision identification consists of the choice of the imaging function from optimality conditions.

Now we turn to the issue of discretization which is conceived in a finite (or boundary) element context with continuous elements. For a discretization parameter $h \in \mathbb{R}_+$ corresponding to a meshing of the test domain Ω, we start with the discretized inputs $D^{(h,\text{input})}$ given on the mesh G_h over the computational domain Ω_h. This leads to the discretized outputs determined by the mapping $\mathcal{M} : (D^{(h,\text{input})}, \omega_{\varepsilon^\star}^\star(x^\star)) \mapsto D^{(h,\text{input})}$. Discretization of the imaging function $\mathcal{I}$ in (2.1) associates the mapping $\mathcal{I}^h : \mathcal{D} \mapsto C(\Omega_h)$ of the discretized data $D^h = (D^{(h,\text{input})}, D^{(h,\text{output})}) \in \mathcal{D}$ with an image I^h which is continuous over Ω_h.

In contrast to our reference example, discretization of an underlying state problem results, generally, in infeasible images. Indeed, for the conventional discretization I_i^h of proper images I_i, $i = 1, \ldots, L$, from (2.4), if $I_i^h \neq I_i$, then, generally, $Z(I_i^h) \neq Z(I_i)$ and $\chi^\star \not\subset Z(I_i^h)$. We note that $Z(I_i) \neq \emptyset$ does not guarantee even nonemptiness $Z(I_i^h) \neq \emptyset$. Therefore, we adapt the criterion of identifiability (2.4) to infeasible images caused by discretization as follows.

DEFINITION 2.4. *Let $\omega_{\varepsilon^\star}^\star(x^\star)$ in $\mathbb{R}^d$ be a parent object with associated child $\chi^\star$ of codimension m which is identifiable according to (2.4). Then the approximation χ^h is called proper, if there exist $1 \leq L \leq d$ nonempty pairwise different nontrivial images $I_i^h = \mathcal{I}^h(D_i^h)$, $i = 1, \ldots, L$, with a nonempty intersection of its zero sets*

$$(2.6) \qquad \bigcap_{i=1}^{L} Z(I_i^h) := \chi^h, \quad I_i^h = \mathcal{I}^h(D_i^h),\ i = 1, \ldots, L,$$

and χ^h has codimension $0 \leq m \leq d$ in $\mathbb{R}^d$.

We note that, if the discretization is confirming that $Z(I_i^h) = Z(I_i)$ for $i = 1, \ldots, L$ in (2.4) and (2.6), then from Definitions 2.3 and 2.4 it follows that $\chi^h = \chi^\star$. Otherwise we can introduce a quality of approximation of $\chi^\star$ by χ^h with the help of a suitable measure satisfying the Hausdorff distance of $\chi^h - \chi^\star$ which can be bounded by an h-dependent error function.

In the stochastic case, the (discrete) data $D^{(h,\sigma)}$ are subject to noise with the standard deviation σ. Following Definition 2.4 we look for a nonempty approximation $\chi^{(h,\sigma)}$ of the child test object $\chi^\star$ of codimension $0 \leq m \leq d$ in $\mathbb{R}^d$ deduced from $1 \leq L \leq d$ pairwise different nontrivial images as

$$(2.7) \qquad \chi^{(h,\sigma)} := \bigcap_{i=1}^{L} Z(I_i^{(h,\sigma)}), \quad I_i^{(h,\sigma)} = \mathcal{I}^{(h,\sigma)}(D_i^{(h,\sigma)}),\ i = 1, \ldots, L.$$

For the example problem of center identification, thus $\chi^\star := x^\star$, a detailed numerical analysis of the error will be reported in section 3.5. For comparison, various identification algorithms reported in [7] for $\sigma = 30\%$ Gaussian noise level have the error ranging from 1 to 25% with respect to the diameter of the test domain. In our numerical tests we observed typically less than 1% error on reasonable meshes. This fact demonstrates high stability with respect to the noise and discretization errors of our identification algorithm, which will be introduced in section 3 based on optimality conditions and zero sets of multiple images.

Our concept here has a broad scope, nevertheless, its particular realizations are different depending on the underlying problem. In the following we specify our concept in detail for the model Helmholtz problem. From optimality conditions of the respective objective functional we derive the imaging function which is suitable for high precision identification of the center of an arbitrary geometric object under unknown boundary conditions. For its numerical implementation we suggest an original Petrov–Galerkin-based enrichment method within generalized FEM, which will be the subject of a forthcoming paper. We observe that it improves significantly the accuracy of discretization in comparison with the standard solvers of the Helmholtz equation; see [55].

3. The Helmholtz problem for identification of the object center from boundary measurements. Here we identify the center of a test object. This task is of primary importance for applications. While the general formulation of the direct and inverse problems is carried out in arbitrary spatial dimensions, a rigorous

asymptotic analysis will be given in 2 dimensions. The 3 dimensional (3d) and one dimensional (1d) cases are considered when analyzing well posedness and numerical stability of the resulting identification algorithm.

3.1. The direct Helmholtz problem. We start with a geometric description of the trial objects (inclusion, obstacle).

Let $\omega \subset \mathbb{R}^d$, $d = 1, 2, 3$, be a generic geometric shape. We assume that $\omega \subset B_1(0)$ and the unit ball $B_1(0)$ is the minimum enclosing ball centered at 0. Moreover, for the asymptotic analysis below we require that $0 \in \omega$. We assume that the boundaries $\partial\omega$ and $\partial\Omega$ are piecewise Lipschitz, which is common in variational formulations. Rescaling ω by a size parameter $\varepsilon > 0$, it produces admissible inclusions $\omega_\varepsilon(x_0) = \{x \in \mathbb{R}^d : \frac{x-x_0}{\varepsilon} \in \omega\} \subset \Omega$ posed at a trial center x_0 in the reference domain Ω. The geometric variables $(\omega, \varepsilon, x_0) \in \Theta = (\Theta_\omega, \Theta_\varepsilon, \Theta_x) \subset \mathbb{R}^d \times \mathbb{R}_+ \times \mathbb{R}^d$ should satisfy the consistency condition $\omega_\varepsilon(x_0) \subset \Omega$. Such admissible geometries $(\omega, \varepsilon, x_0) \in \Theta$ will be used further for the sake of variation of topology of the reference domain. For the direct problem, we fix $\omega_\varepsilon(x_0)$ in Ω.

As a reference model we consider the scalar, complex-valued Helmholtz equation

$$(3.1) \qquad -(\Delta + k^2)u = 0 \quad \text{in } \Omega \setminus \overline{\omega_\varepsilon(x_0)},$$

with Neumann condition at the external boundary

$$(3.2) \qquad \frac{\partial u}{\partial n} = g \quad \text{on } \partial\Omega,$$

and Robin condition at the (internal) boundary of the inclusion

$$(3.3) \qquad \frac{\partial u}{\partial n} + \alpha u = 0 \quad \text{on } \partial\omega_\varepsilon(x_0).$$

Here the Neumann data $g \in L^2(\partial\Omega; \mathbb{C})$, the wave number $k \in \mathbb{R}$, and the surface impedance $\alpha \in L^\infty(\partial\omega; \mathbb{C})$ are given, and n denotes the normal vector at the boundary. Since the function $\alpha(y)$ is given for $y \in \partial\omega$, after stretching $y = \frac{x-x_0}{\varepsilon}$, the value of α in (3.3) means $\alpha(\frac{x-x_0}{\varepsilon})$ for $x \in \partial\omega_\varepsilon(x_0)$. In the following $x \in \mathbb{R}^d$ refers to the reference domain Ω, and $y \in \mathbb{R}^d$ to the stretched domain ω.

We note that, on the one hand, a Robin boundary condition (3.3) implies approximation of the Neumann condition $\frac{\partial u}{\partial n} = 0$ (the sound hard obstacle) in the case of small $|\alpha| \to 0$ (see [27]). On the other hand, in the case $|\alpha| \to \infty$ relation (3.3) corresponds to a penalized version of the Dirichlet condition $u = 0$ (the sound soft obstacle). In this way problem (3.1)–(3.3) accounts for arbitrary boundary conditions depending on the parameter α.

The weak formulation of (3.1)–(3.3) reads: Find $u^{(\omega,\varepsilon,x_0,\alpha)} \in H^1(\Omega \setminus \overline{\omega_\varepsilon(x_0)}; \mathbb{C})$ such that

$$(3.4) \quad \begin{aligned} &\int_{\Omega\setminus\omega_\varepsilon(x_0)} (\nabla u^{(\omega,\varepsilon,x_0,\alpha)} \cdot \nabla\overline{v} - k^2 u^{(\omega,\varepsilon,x_0,\alpha)}\overline{v})\, dx + \int_{\partial\omega_\varepsilon(x_0)} \alpha u^{(\omega,\varepsilon,x_0,\alpha)}\overline{v}\, dS_x \\ &= \int_{\partial\Omega} g\overline{v}\, dS_x \quad \text{for all } v \in H^1(\Omega \setminus \overline{\omega_\varepsilon(x_0)}; \mathbb{C}), \end{aligned}$$

where we mark the dependence of the geometric and physical variables $(\omega, \varepsilon, x_0, \alpha)$. Problem (3.4) can be expressed equivalently with the help of the Cherkaev–Gibiansky variational principle:

$$(3.5) \qquad \underset{\text{Re}(v)}{\text{minimize}} \, \underset{\text{Im}(v)}{\text{maximize}} \, L(v) \quad \text{over } v \in H^1(\Omega \setminus \overline{\omega_\varepsilon(x_0)}; \mathbb{C})$$

with the Lagrangian $L : H^1(\Omega \setminus \overline{\omega_\varepsilon(x_0)}; \mathbb{C}) \mapsto \mathbb{R}$ of the form

(3.6)
$$L(v) := \operatorname{Re} \left\{ \tfrac{1}{2} \int_{\Omega \setminus \omega_\varepsilon(x_0)} (\nabla v \cdot \nabla v - k^2 v^2) \, dx + \tfrac{1}{2} \int_{\partial \omega_\varepsilon(x_0)} \alpha v^2 \, dS_x - \int_{\partial \Omega} g v \, dS_x \right\}.$$

The optimality system (3.4) is a necessary condition for the minimax problem (3.5). Under reasonable assumptions on k and α (see [17, 24]), there exists a (unique) solution of the variational equation (3.4). Summarizing these assumptions, k should not be too large, and α should be either not too large or it should have a definite sign such that $\operatorname{Re}(\alpha) \geq 0$ and $\operatorname{Im}(\alpha) \geq 0$ or $\operatorname{Im}(\alpha) \leq 0$ uniformly at $\partial \omega$. The latter case allows the Dirichlet boundary condition in the limit of $|\alpha| \to \infty$. For fixed k, we define the admissible set $\Theta_\alpha \subset L^\infty(\partial \omega; \mathbb{C})$ of such α which allow solvability of (3.4).

3.2. The inverse problem of object identification. In the inverse setting of the problem, the shape $\omega^\star$, size $\varepsilon^\star$, and position $x^\star$ for an unknown geometric object, and the surface impedance $\alpha^\star$ are to be identified and reconstructed from the known boundary measurement(s) $u^\star = u^{(\omega^\star, \varepsilon^\star, x^\star, \alpha^\star)}$ at $\partial \Omega$. For this purpose, a trial object $\omega_\varepsilon(x_0)$ is put in Ω such that $(\omega, \varepsilon, x_0) \in \Theta = (\Theta_\omega, \Theta_\varepsilon, \Theta_x)$ are admissible. Using an admissible trial surface impedance parameter $\alpha \in \Theta_\alpha$ we find a family of solutions $u^{(\omega, \varepsilon, x_0, \alpha)}$ of problem (3.4). The admissible set $\widetilde{\Theta} := (\Theta_\omega, \Theta_\varepsilon, \Theta_x, \Theta_\alpha)$ was discussed before. For the trial variables $(\omega, \varepsilon, x_0, \alpha) \in \widetilde{\Theta}$ we consider the usual square function of the misfit at $\partial \Omega$

(3.7)
$$J(\omega, \varepsilon, x_0, \alpha) := \tfrac{1}{2} \int_{\partial \Omega} |u^{(\omega, \varepsilon, x_0, \alpha)} - u^\star|^2 \, dS_x$$

as the objective function for the topology optimization problem:

(3.8)   minimize $J(\omega, \varepsilon, x_0, \alpha)$ over admissible $(\omega, \varepsilon, x_0, \alpha) \in \widetilde{\Theta}$ subject to (3.4).

If the test variables satisfy $(\omega^\star, \varepsilon^\star, x^\star, \alpha^\star) \in \widetilde{\Theta}$, then this is the argument of the trivial minimum in (3.8).

In the following we bring (3.7) into a form which is suitable for asymptotic analysis. We start with primal-dual arguments. Since $u^{(\omega, \varepsilon, x_0, \alpha)}$ denotes the primal state variable, a dual state variable $v^{(\omega, \varepsilon, x_0, \alpha)}$ can be obtained with the help of a Fenchel–Legendre duality corresponding to the following variational principle:

(3.9) $\min\limits_{\operatorname{Re}(u), \operatorname{Re}(v)} \max\limits_{\operatorname{Im}(u), \operatorname{Im}(v)} \mathcal{L}(u, v)$ over $u, v \in H^1(\Omega \setminus \overline{\omega_\varepsilon(x_0)}; \mathbb{C})$,

where the Lagrangian $\mathcal{L}$ has the form (compare with (3.6))

(3.10)
$$\mathcal{L}(u, v) := \operatorname{Re} \left\{ \tfrac{1}{2} \int_{\Omega \setminus \omega_\varepsilon(x_0)} (\nabla u \cdot \nabla v - k^2 uv) \, dx + \tfrac{1}{2} \int_{\partial \omega_\varepsilon(x_0)} \alpha uv \, dS_x - \int_{\partial \Omega} gv \, dS_x \right.$$
$$\left. + \tfrac{1}{2} \int_{\partial \Omega} (u - u^\star)^2 \, dS_x \right\}.$$

The first order optimality conditions for (3.9) yield (3.4) together with the dual vari-

ational problem: Find $v^{(\omega,\varepsilon,x_0,\alpha)} \in H^1(\Omega \setminus \overline{\omega_\varepsilon(x_0)}; \mathbb{C})$ such that

$$
(3.11) \qquad \int_{\Omega \setminus \omega_\varepsilon(x_0)} (\nabla v^{(\omega,\varepsilon,x_0,\alpha)} \cdot \nabla \overline{u} - k^2 v^{(\omega,\varepsilon,x_0,\alpha)}\overline{u})\, dx + \int_{\partial \omega_\varepsilon(x_0)} \alpha v^{(\omega,\varepsilon,x_0,\alpha)}\overline{u}\, dS_x
$$
$$
= -\int_{\partial\Omega} (u^{(\omega,\varepsilon,x_0,\alpha)} - u^\star)\overline{u}\, dS_x \quad \text{for all } u \in H^1(\Omega \setminus \overline{\omega_\varepsilon(x_0)}; \mathbb{C}),
$$

which is analogous to problem (3.4) and differs from it by the Neumann data at $\partial\Omega$.

In the reference domain Ω without inclusion, from (3.4) and (3.11) as $\varepsilon = 0$ we define the background solutions of the respective primal and dual problems: Find $u^0 \in H^1(\Omega; \mathbb{C})$ such that

$$
(3.12) \qquad \int_{\Omega} (\nabla u^0 \cdot \nabla \overline{v} - k^2 u^0 \overline{v})\, dx = \int_{\partial\Omega} g\overline{v}\, dS_x \quad \text{for all } v \in H^1(\Omega; \mathbb{C}),
$$

and $v^0 \in H^1(\Omega; \mathbb{C})$ such that

$$
(3.13) \qquad \int_{\Omega} (\nabla v^0 \cdot \nabla \overline{u} - k^2 v^0 \overline{u})\, dx = -\int_{\partial\Omega} (u^0 - u^\star)\overline{u}\, dS_x \quad \text{for all } u \in H^1(\Omega; \mathbb{C}).
$$

The background solutions u^0 and v^0 will be used for construction of the imaging function I.

With the help of (3.12) and (3.13), subtracting and adding u^0 in (3.7) and using $\frac{\partial v^0}{\partial n} = -(u^0 - u^\star)$ at $\partial\Omega$, we rewrite the objective J equivalently as

$$
(3.14) \qquad J(\omega,\varepsilon,x_0,\alpha) = J_0 - \mathrm{Re}\left\{ \int_{\partial\Omega} (u^{(\omega,\varepsilon,x_0,\alpha)} - u^0)\frac{\partial \overline{v}^0}{\partial n}\, dS_x \right\}
$$
$$
+ \tfrac{1}{2}\int_{\partial\Omega} |u^{(\omega,\varepsilon,x_0,\alpha)} - u^0|^2\, dS_x, \quad J_0 := \tfrac{1}{2}\int_{\partial\Omega} |u^0 - u^\star|^2\, dS_x.
$$

We note that J_0 in the right-hand side of (3.14) is constant with respect to the trial variables $(\omega, \varepsilon, x_0, \alpha)$. Relying on small geometric objects, we can apply asymptotic arguments to (3.14) and expand J in small ε. While the asymptotic expansion is somewhat known in the literature for the specific cases of boundary conditions of Dirichlet, Neumann, and Robin type with α constant, here we get the result for arbitrary, constant, or distributed parameter α of the surface impedance. It allows us to treat a priori unknown boundary conditions of the test object.

To obtain the asymptotic expansion for arbitrary shapes and unknown boundary conditions we generalize the methods of singular perturbations with variational arguments. This results in a two-scale expansion of the state problem. One asymptotic series is given by solutions of variational problems in the reference domain Ω. The second asymptotic series can be expressed by harmonics with respect to the stretched variable $y = \frac{x - x_0}{\varepsilon}$ in the exterior domain $\mathbb{R}^d \setminus \overline{\omega}$. The construction is related closely to Green functions; see [33]. We endow it with a variational formulation using the nontrivial kernel of exterior Laplace problems in weighted Sobolev spaces; see [15]. In particular, we obtain the far field pattern which contains the geometric information of the test object. In the present paper we confine ourselves to the first order asymptotic information which suffices to identify the center of an object. We emphasize that the rigorous justification of such expansions is itself a hard task with a huge number of fine asymptotic calculations.

For two spatial dimensions ($d = 2$), we rigorously justify in Appendix A the following representation as $\varepsilon \searrow +0$,

$$(3.15) \quad \begin{aligned} J(\omega, \varepsilon, x_0, \alpha) = J_0 + 2\pi\varepsilon \operatorname{Re}\{\langle\alpha\rangle u^0(x_0)\overline{v^0}(x_0)\} \\ + \operatorname{O}\big((1 + \|\alpha\|_\infty + \|\alpha\|_\infty^2 \varepsilon)^2 \varepsilon^2\big), \end{aligned}$$

where u^0 and v^0 are the solutions of (3.12) and (3.13), the notation $\langle\alpha\rangle$ stands for the average of α over $\partial\omega$, and $\|\cdot\|_\infty$ stands for the L^∞-norm. For convenience we represent the first order asymptotic term in (3.15) equivalently as

$$(3.16) \quad \operatorname{Re}\{\langle\alpha\rangle u^0(x_0)\overline{v^0}(x_0)\} = \operatorname{Re}\langle\alpha\rangle \operatorname{Re}\{u^0(x_0)\overline{v^0}(x_0)\} - \operatorname{Im}\langle\alpha\rangle \operatorname{Im}\{u^0(x_0)\overline{v^0}(x_0)\}.$$

Using the asymptotic representation (3.15), we next derive optimality conditions for the topology optimization problem (3.8), which will be used further for high precision imaging.

3.3. The optimality-condition-based imaging of the center. In the standard approach, the admissible set of parameters $\alpha \in \Theta_\alpha$ is avoided according to either the Neumann condition by $\alpha = 0$ or the Dirichlet condition by $|\alpha| \to \infty$, which is predefined. In the former case, the leading first order asymptotic term in (3.15) disappears. In the latter case, if $|\operatorname{Im}(\alpha)| \to \infty$ and the real part is chosen as $\operatorname{Re}(\alpha) = \frac{1}{-\varepsilon \ln(\varepsilon \operatorname{cap}(\omega))} + \operatorname{O}(\frac{1}{\varepsilon|\ln\varepsilon|^2})$, then (3.15) tends to the expression for the Dirichlet case (when $d = 2$)

$$J(\omega, \varepsilon, x_0) = J_0 + \frac{2\pi}{-\ln(\varepsilon \operatorname{cap}(\omega))}\operatorname{Re}\{u^0(x_0)\overline{v^0}(x_0)\} + \operatorname{O}\left(\frac{1}{|\ln\varepsilon|^2}\right).$$

We note that in both cases when boundary conditions of the trial objects (and, respectively, of the test object) are set a priori, the complementary term $\operatorname{Im}\langle\alpha\rangle \cdot \operatorname{Im}\{u^0(x_0)\overline{v^0}(x_0)\}$ in (3.16) does not appear in the subsequent optimization.

Differently from the above consideration, we assume the trial coefficient $\alpha \in \Theta_\alpha$ to be unknown a priori. For the test variables $(\omega^\star, \varepsilon^\star, x^\star, \alpha^\star) \in \widetilde{\Theta}$ chosen arbitrarily, definition (3.7) suggests the optimality

$$J(\omega^\star, \varepsilon^\star, x^\star, \alpha^\star) = 0 \leq J(\omega, \varepsilon, x_0, \alpha) \quad \text{for all } (\omega, \varepsilon, x_0, \alpha) \in \widetilde{\Theta}.$$

In particular, for all admissible constants $\alpha^\star$ and small ε, it holds due to (3.15) that

$$(3.17) \quad \begin{aligned} J(\omega^\star, \varepsilon^\star, x^\star, \alpha^\star) = 0 \leq J(\omega^\star, \varepsilon, x^\star, \alpha^\star) = J_0 + 2\pi\varepsilon\big\{\operatorname{Re}(\alpha^\star)\operatorname{Re}\{u^0(x^\star)\overline{v^0}(x^\star)\} \\ - \operatorname{Im}(\alpha^\star)\operatorname{Im}\{u^0(x^\star)\overline{v^0}(x^\star)\}\big\} + \operatorname{O}\big((1 + |\alpha^\star| + |\alpha^\star|^2\varepsilon)^2\varepsilon^2\big). \end{aligned}$$

For the Dirichlet case, when $\omega^\star, \varepsilon^\star, x^\star$ are fixed and $\operatorname{Im}(\alpha^\star) \to +\infty$ or $\operatorname{Im}(\alpha^\star) \to -\infty$, the complementary terms to $\operatorname{Im}(\alpha^\star)$ by arbitrary ε in (3.17) should be zero. Thus we arrive at the optimality condition of the form

$$(3.18) \quad \operatorname{Im}\{u^0(x^\star)\overline{v^0}(x^\star)\} = 0,$$

which is necessary for the Dirichlet case. We therefore argue the following result.

THEOREM 3.1. *The center $x^\star$ of a sound soft test object $\omega^\star_{\varepsilon^\star}(x^\star) \subset \mathbb{R}^2$ of arbitrary shape $\omega^\star$ and size $\varepsilon^\star$ satisfies the necessary optimality condition* (3.18), *where u^0 and v^0 are the primal and dual background solutions of problems* (3.12) *and* (3.13), *respectively.*

The assertion of Theorem 3.1 is validated also numerically in section 3.4. We emphasize that, in spite of the asymptotic arguments of the small trial sizes ε which were used, the size $\varepsilon^\star$ of the test object does not need to be small.

Now we relate the specific result of center identification obtained for the Helmholtz problem to the abstract concept of object imaging from section 2. For the input $D^{\text{input}} = \{\Omega, k, g\}$, the synthetic output $D^{\text{output}} = \{u^\star : u^\star = u^{(\omega^\star, \varepsilon^\star, x^\star, \alpha^\star)} \text{on } \partial\Omega\}$ is obtained by solving the direct Helmholtz problem (3.4) for the known test object $\omega^\star_{\varepsilon^\star}(x^\star)$ with the known surface impedance $\alpha^\star$. This solution synthesizes the measurement $\mathcal{M} : (D^{\text{input}}, \omega^\star_{\varepsilon^\star}(x^\star)) \mapsto D^{\text{output}}$. Based on (3.18) we define the imaging function $\mathcal{I} : \mathcal{D} = \{D : D = (D^{\text{input}}, D^{\text{output}})\} \mapsto C(\Omega)$ through the following image

$$(3.19) \qquad I = \mathcal{I}(D), \quad I(x) := \text{Im}\{u^0(x)\overline{v^0}(x)\} \quad \text{for } x \in \Omega.$$

From Theorem 3.1 and (3.18) we infer the following result.

PROPOSITION 3.2. *Every image of $\mathcal{I}$ in* (3.19) *is feasible with respect to the center $x^\star$ of a sound soft test object $\omega^\star_{\varepsilon^\star}(x^\star) \subset \mathbb{R}^2$ according to Definition 2.2, that is, $x^\star \in Z(I)$ for the zero set Z of the imaging function I in* (3.19).

Using Proposition 3.2, the necessary criterion (2.5) from section 2 can be applied in the continuous setting to identify the center $x^\star$ from the intersection of $1 \leq L \leq d$ feasible images I_i of pairwise different data D_i, $i = 1, \ldots, L$, in (3.19). Nevertheless, our aim is to construct a numerical algorithm for the efficient solution of the identification problem after discretization. Therefore, we next discuss the capability of the optimality condition (3.18) and the respective imaging function (3.19) to identify the center of a test object in discrete spaces. In the following we will verify numerically that criterion (3.18) in its discrete version holds true in all spatial dimensions (≤ 3) and for all boundary conditions of the test object providing us with either the exact center $x^\star$ or its close approximation.

The principal difficulty of discretization here concerns singular perturbations. The asymptotic analysis passing the object size $\varepsilon \searrow +0$, which was argued here in a continuous setting, is less evident in finite dimensions. Indeed, after discretization of the underlying problem on a finite element mesh we cannot pass the object size $\varepsilon \searrow +0$ within a sole element. This difficulty is connected closely with the spatial dimensionality. Let us first consider the 1d case and let the test domain $\Omega = (A, B)$, $A < B$. The test object is represented by a point $x^\star \in (A, B)$. We prove the following result.

THEOREM 3.3. *Consider the test point $x^\star \in (A, B) \subset \mathbb{R}^1$ subject to homogeneous either Dirichlet or Neumann boundary conditions, which is illuminated with the wave $g(x) = e^{ikx}$. Then $x^\star$ coincides with a zero point x_0 such that $I(x_0) = 0$ for the imaging function I defined in* (3.19) *and for the wave numbers $k = \frac{\pi(\frac{1}{2}+n)}{B-A}$, $n \in \mathbb{N}$. The zero point $x_0 = x^\star$ is unique only if $n = 0$.*

Proof. First, we construct analytically the exact solutions $u^\star$. For the Dirichlet condition $u^\star(x^\star) = 0$, the Helmholtz problem

$$(3.20) \quad u^\star_{xx}(x) + k^2 u^\star(x) = 0 \text{ for } x \in (A, B) \setminus \{x^\star\}, \quad u^\star_x(x) = ike^{ikx} \text{ for } x = A, B,$$

admits the following (unique) solution

$$u^\star(x) = -ie^{ikA} \tfrac{\sin k(x^\star-x)}{\sin k(x^\star-A)} \text{ for } x \in [A, x^\star], \; u^\star(x) = ie^{ikB} \tfrac{\sin k(x-x^\star)}{\sin k(B-x^\star)} \text{ for } x \in [x^\star, B].$$

Similarly, for the Neumann condition $u^\star_x(x^\star) = 0$, the solution of (3.20) has the form

$$u^\star(x) = ie^{ikA} \tfrac{\cos k(x^\star-x)}{\sin k(x^\star-A)} \text{ for } x \in [A, x^\star], \; u^\star(x) = -ie^{ikB} \tfrac{\cos k(x-x^\star)}{\sin k(B-x^\star)} \text{ for } x \in [x^\star, B].$$

Second, for the background solution (the wave) $u^0(x) = e^{ikx}$, $x \in [A, B]$, of (3.12), its dual can be calculated from (3.13) as

$$v^0(x) = -\frac{(u^\star(A) - u^0(A)) \cos k(B-x) + (u^\star(B) - u^0(B)) \cos k(x-A)}{k \sin k(B-A)} \text{ for } x \in [A, B].$$

Substituting the expressions of u^0 and v^0 into (3.19), we calculate the image $I(x)$ for $x \in (A, B)$. In both cases of the Dirichlet and Neumann conditions we find that $I(x_0) = 0$ for $\cos 2k(x_0 - x^\star) = 1$, $\sin 2k(x_0 - x^\star) = 0$, and $\cos k(B - A) = 0$. Henceforth, with the wave numbers $k = \frac{\pi(\frac{1}{2}+n)}{B-A}$, $n \in \mathbb{N}$, the zero points are $x_0 = x^\star + \frac{\pi l}{k}$, $l \in \mathbb{N}$. This proves the assertion. $\quad\square$

The above analysis of the 1d identification problem will hint at numerical issues of the imaging with $\mathcal{I}$ from (3.19) in 2 and 3 dimensions.

3.4. The identification algorithm and numerical issues. We start by explaining the discretization.

The data of the problem are discretized on a mesh G_h over the computational domain Ω_h associated with Ω. A uniform quadrilateral mesh in 2 dimensions (respectively, polyhedral in 3 dimensions) of the mesh size h is used. Discrete solutions of the Helmholtz problems (3.4), (3.12), and (3.13) in Ω_h are indicated by a subscript h. It is known that generalized finite element methods (GFEM) are well suited for the numerical solution of Helmholtz problems. We refer to [55] for an overview. Within GFEM, we utilize a particular realization, which here is bilinear in 2 dimensions and trilinear in 3 dimensions, based on a Petrov–Galerkin enrichment (PGE). The usual linear basis is used for trial functions, while test functions are enriched with hierarchical shape functions based on Gegenbauer polynomials. The respective quadratic basis of the test functions is obtained from a dispersion analysis. We note that the system matrix is symmetric in this case which is numerically advantageous. From our a priori and a posteriori numerical analysis we report that the PGE approximates the linear interpolate of the exact solution with order $o((kh)^7)$. This implies highly accurate approximation in comparison with the standard Galerkin least-squares (GLS) method which has order $O((kh)^2)$.

We formulate an identification algorithm for the specific case of illumination with plane waves, which can be adapted to other physical situations, too. For the Helmholtz problem (3.4) in $\mathbb{R}^d$, $d = 1, 2, 3$, we specify the inputs $D^{\text{input}} = \{\Omega, k, g\}$ with specific Neumann data g given at $\partial\Omega$ by

$$(3.21) \quad \begin{aligned} & g(x) = e^{ikx} \text{ for } d = 1, \quad g(x) = e^{ik(x_1 \cos\theta_1 + x_2 \sin\theta_1)} \text{ for } d = 2, \\ & g(x) = e^{ik(x_1 \cos\theta_1 \sin\theta_2 + x_2 \sin\theta_1 \sin\theta_2 + x_3 \cos\theta_2)} \text{ for } d = 3, \quad (i^2 = -1). \end{aligned}$$

Here θ denotes the incident angle. It is $\theta = 1$ for $d = 1$, and $\theta = (\theta_1, \ldots, \theta_{d-1})$ for $d > 1$. The associated output $D^{\text{output}} = \{u^\star \text{ on } \partial\Omega\}$ of g is "measured" due to scattering by the test obstacle $\omega_{\varepsilon^\star}^\star(x^\star)$ in Ω. Henceforth, for fixed domain Ω and wave number k, the data $D = (D^{\text{input}}, D^{\text{output}})$ are determined by the parameter $\theta \in \mathbb{R}^{\max(1, d-1)}$ in (3.21). After discretization of the problem in the computational domain Ω_h, for the discrete Neumann data g_h and measurement $u_h^\star$ at $\partial\Omega_h$ we formulate the following algorithm.

ALGORITHM 3.4. *Fix the wave number k and the computational domain Ω_h endowed with a mesh of size h. Set pairwise different incident angles $\theta^{(1)}, \ldots, \theta^{(d)} \in \mathbb{R}^{d-1}$, if $d > 1$. Otherwise, set $\theta^{(1)} = 1$ in 1 dimension.*

Step 1. For $i = 1, \ldots, d$, set $\theta = \theta^{(i)}$ and determine the respective g_h at $\partial\Omega_h$ according to (3.21). Repeat Steps 2–6.

Step 2. *Determine the (measured) output data $u_h^\star$ at $\partial\Omega_h$ on the basis of g_h and θ.*

Step 3. *Calculate the background solution u_h^0 of (3.12) with the Neumann data g_h.*

Step 4. *Calculate the adjoint solution v_h^0 of (3.13) with the Neumann data $u_h^\star - u_h^0$ at $\partial\Omega_h$.*

Step 5. *Calculate the (discretized) imaging function from (3.19) as*

$$(3.22) \qquad I_i^h(x) = \mathrm{Im}\{u_h^0(x)\overline{v_h^0}(x)\} \quad \text{for } x \in \Omega_h.$$

Step 6. *Find the zero set*

$$(3.23) \qquad Z(I_i^h) = \{x \in \Omega_h : I_i^h(x) = 0\}.$$

Save $Z(I_i^h)$. If $i < d$, then set $i = i + 1$ and go to Step 1.

Step 7. *Determine the approximate center x^h of the test object as the intersection of d zero sets:*

$$(3.24) \qquad x^h = \bigcap_{i=1}^{d} Z(I_i^h).$$

We stress that (3.23) in Step 6 and (3.24) in Step 7 are given in accordance with Definition 2.4 of the proper approximation of the test object from section 2. Below we discuss the numerical realization of Algorithm 3.4.

For numerical tests, in Step 2 we use the synthetic data $u_{\widetilde{h}}^{(\omega^\star,\varepsilon^\star,x^\star,\alpha^\star)}$ to get the measurement $u_h^\star$ at $\partial\Omega_h$. We obtain $u_{\widetilde{h}}^{(\omega^\star,\varepsilon^\star,x^\star,\alpha^\star)}$ by solving numerically the Helmholtz problem (3.4) in the computational domain $\Omega_{\widetilde{h}} \setminus \omega_{\varepsilon^\star}^\star(x^\star)$ with the test object $\omega_{\varepsilon^\star}^\star(x^\star)$, surface impedance $\alpha^\star$, and Neumann data $g_{\widetilde{h}}$ given at $\partial\Omega_{\widetilde{h}}$ by (3.21) with $\theta = \theta^{(i)}$ for $i = 1,\ldots,d$. The meshes for computing in $\Omega_{\widetilde{h}}$ and in Ω_h are, generally, not the same. Typically, we used hierarchical meshes with $\widetilde{h} \le h$.

Zero sets in (3.23) and (3.24) are realized by the narrow band technique; see, for instance, [44] and the references therein. In a narrow band of nodes near $Z(I^h)$ we utilize the quadratic approximation of the imaging function I^h due to its specific structure (3.22) as the product of two functions, which are discretized by linear finite elements. A linear approximation of I^h over the quadrilateral elements can be applied, too, but it is slightly less accurate. As a result we find the discrete zero set $Z^h(I^h)$ on a local grid which is, generally, different from the computational grid G_h in Ω_h.

In the following we report on our numerical findings. We realize the example configuration of $\Omega_h = \Omega$ given by the unit square in 2 dimensions and the unit cube in 3 dimensions.

For 2 dimensions, the numerical result of Algorithm 3.4 for a sound soft obstacle is depicted in Figure 2. The dotted lines present discrete zero sets $Z^h(I^h)$ due to the narrow band realization of $Z(I^h)$. In the plots of Figures 2(a) and (b), the point obstacle $\omega_{\varepsilon^\star}^\star(x^\star) = x^\star = (0.25, 0.375)$, which is marked with the blue solid point, is illuminated by the plane waves of the form (3.21) with various incident angles θ. The single image for $\theta = 0$ is depicted in the plot (a). The point $x^\star$ lies exactly in the segment $Z(I^h)$ yielding the zero set in (3.23). Multiple images corresponding to $\theta \in \{0, \frac{\pi}{6}, \frac{\pi}{3}, \frac{\pi}{2}, \frac{2\pi}{3}, \frac{5\pi}{6}\}$ are presented in the plot (b). We observe clearly that the test point $x^\star$ is identified exactly as the intersection x^h of any two segments $Z(I_i^h)$, $i = 1, 2$. This corresponds to the imaging under double measurements with two different incident angles $\theta^{(1)}$ and $\theta^{(2)}$ according to Step 7 in the identification algorithm.

The result of Algorithm 3.4 for a fish-shaped junk of geometric objects of different dimensions $\omega_{\varepsilon^\star}^\star(x^\star)$ is depicted in Figure 2(c). The two plane waves with $\theta^{(1)} = \frac{\pi}{8}$
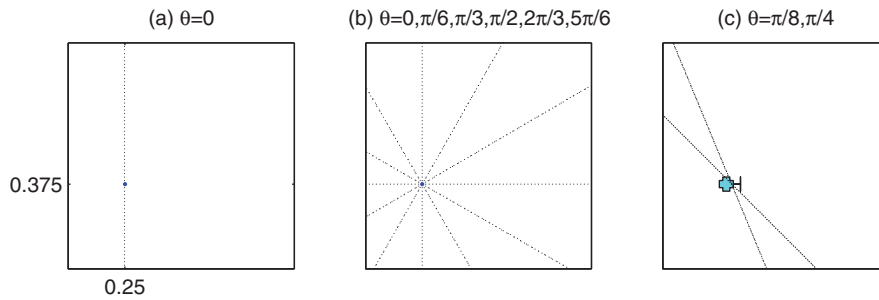
FIG. 2. *Identification of sound soft obstacles from multiple images in* 2 *dimensions.*

and $\theta^{(2)} = \frac{\pi}{4}$ determine uniquely the intersection point x^h as shown here. This point corresponds to the center of the union of mesh points representing the test object $\omega_{\varepsilon^\star}^\star(x^\star)$.

From our numerical tests we can report that the identification of the object center holds true for a variety of test objects of arbitrary geometry and size. This is in accordance with Theorem 3.1.

In 3 dimensions, the result of Algorithm 3.4 for a point shaped sound soft obstacle was presented earlier in Figure 1 in section 2.

We emphasize that the identification $x^h = x^\star$ is exact (!) in the ideal situation when the test point $x^\star$ coincides with nodes of the mesh Ω_h, which was tested for mesh sizes in the range of $h \in \{2^{-8}, \ldots, 2^{-3}\}$. Otherwise, we report the numerical error $|x^h - x^\star| = O(h^4)$. To the best of our knowledge, such precise results were not available in the literature.

It is important to report on the uniqueness of identification, which depends on the wave number k. Theorem 3.3 suggests that k should be low enough. In the presented examples of Ω we have fixed $k = \frac{\pi}{2}$. In fact, our numerical results do not depend on k in the range $k \in (0, \frac{\pi}{2} + \delta)$, where δ depends on the geometry. Otherwise, for large k there appear nonunique intersection points x^h in (3.24) due to eigenfrequencies, which produce false results. Theorem 3.3 for the 1d case and our 2 dimensions and 3d numerical tests suggest that $k \in (0, \frac{\pi}{2\mathrm{diam}\Omega})$ is sufficient for identifiability.

When the state problem is perturbed, for example, with noisy data, the straight (planar) structure of zero sets observed in the figures can be destroyed. To restore this geometric property of zero sets, and hence, the accuracy of the algorithm for perturbed data, it is helpful to average the zero set $Z(I^h)$ across the direction of the incident wave. For this purpose we suggest updating $Z(I^h)$ after Step 6 in Algorithm 3.4 in the following way. Let $Q \in \mathbb{R}^{d \times d}$ be an orthogonal matrix of rotation of the reference coordinate system to the local coordinates corresponding to the wavefront in (3.21). For instance, $Q = \begin{pmatrix} \cos\theta_1 & -\sin\theta_1 \\ \sin\theta_1 & \cos\theta_1 \end{pmatrix}$ in $\mathbb{R}^2$.

Step 6'. *Let $z_j \in \mathbb{R}^d$, $j = 1, \ldots, N$, be the points contained in the discrete zero set $Z^h(I^h) =: \{z_j\}_{j=1}^N$. For $j = 1, \ldots, N$, after rotation $Qz_j = ((Qz_j)_1, \ldots, (Qz_j)_d)^\top$, average the first coordinate as $\langle (Qz)_1 \rangle = \frac{1}{N} \sum_{j=1}^N (Qz_j)_1$ and reset the zero set with the averaged points as $Z^h(I^h) := \{Q^\top(\langle (Qz)_1 \rangle, (Qz_j)_2, \ldots, (Qz_j)_d)^\top\}_{j=1}^N$.*

The selected results for $h = 2^{-4}$ after application of Step 6' are depicted in Figures 3(a)–(c) for 10, 25, and 50% noise. The restored zero sets are drawn here with the solid lines in comparison with the dotted lines of the perturbed zero sets which exhibit wavelike distortions. We clearly observe in Figure 3 the improvement, namely, that the restored sets $Z^h(I^h)$ become closer to the test point $x^\star$.
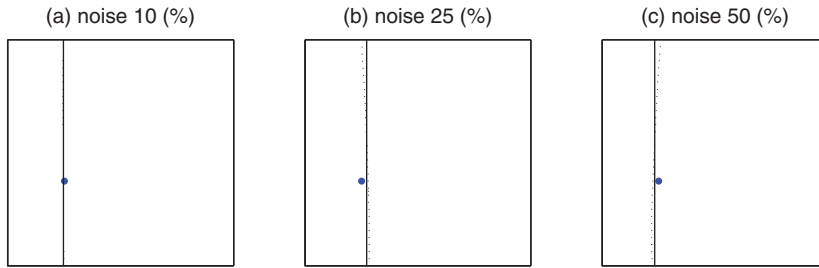
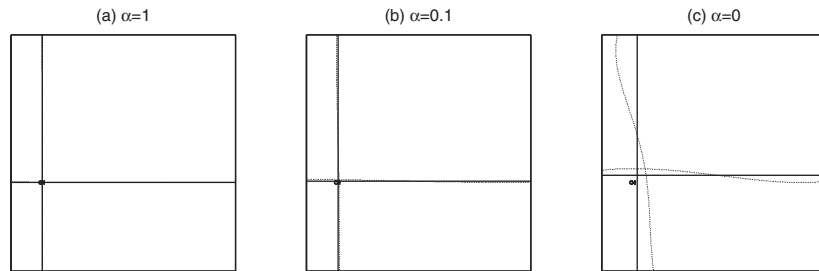FIG. 3. *Restoration of perturbed zero sets with the help of averaging across incident direction.*

FIG. 4. *Imaging under double measurements of a fish-shaped object with the impedance $\alpha^\star$.*

Further we apply the restoration procedure also for a test object under impedance and sound hard boundary conditions. In fact, the identification algorithm is applicable numerically as well to finite $\alpha^\star \in \mathbb{R}$ corresponding to the impedance boundary condition, in particular, to $\alpha^\star = 0$ for the Neumann condition (the sound hard obstacle). The selected numerical results of imaging a fish-shaped junk under double measurements with $\alpha^\star = \{1, 0.1, 0\}$ is depicted in Figures 4(a)–(c), respectively, for $h = 2^{-7}$. We observe that the accuracy of Algorithm 3.4 measured in terms of $|x^h - x^\star|$ is very good for large $\alpha^\star$ (here, for $\alpha^\star \geq 1$), and it becomes less accurate when $\alpha^\star \searrow +0$. The worst case of $\alpha^\star = 0$, depicted in Figure 4(c), corresponds to the Neumann condition. This result still gives an acceptable approximation. We note that to improve the accuracy of the identification of the sound hard obstacle, this case needs to use the second order asymptotic approximation in ε of the objective function in (3.15) which shall allow us to derive a high order imaging function well suitable for the Neumann boundary condition of a test object.

We also test the case of multiple objects posed in the test domain and report the following. The identification algorithm in the outlined frame of illumination by a single plane wave of low frequency does not distinguish between separate objects, but rather it finds the unique point x^h approximating the center (a geometric mean) of the union of mesh points representing these objects. To separate multiple test objects we shall suggest another setting for identification. It must allow high frequencies, for example, based on illumination from multiple point sources.

In the next section we investigate in detail the stability of Algorithm 3.4 with respect to discretization and noisy data.

3.5. Stability of the identification algorithm. For the stability analysis we fix in this section the spatial dimension to be 2 dimensions and rely on the Dirichlet
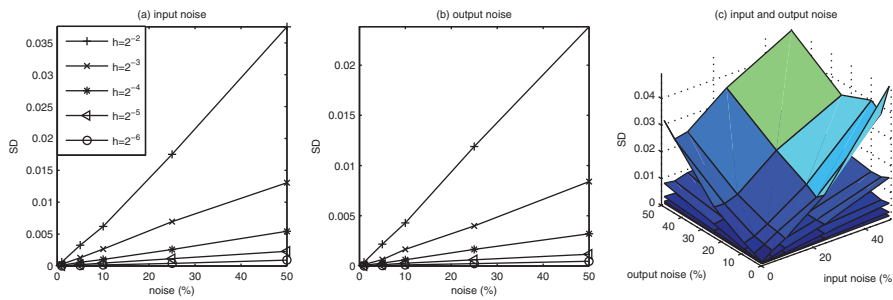
FIG. 5. *Error* $\mathrm{sd}_N|x^{(h,\sigma)} - x^\star|$ *in dependence of noise* σ *for various mesh sizes* h.

boundary condition of a point-shaped object. We start with the stochastic case of noisy data which is of primary interest in practical applications.

We mask data with a Gaussian noise with the standard deviation σ measured in percent with respect to the max-norm of the respective data function. We compute $N = 100$ realizations subject to noise level σ and evaluate the standard deviation (sd) of the distance between the proper approximation $x^{(h,\sigma)}$ obtained from Algorithm 3.4 and the test center $x^\star$. We distinguish the input noise σ_{input} and the output noise σ_{output}. For the underlying problem, σ_{input} is caused by the stochastic Neumann data $g_{(h,\sigma_{\mathrm{input}})}$ given at $\partial\Omega_h$ according to (3.21). The input noise is applied when solving the Helmholtz problems in Steps 2 and 3. The output noise σ_{output} is a consequence of the stochastic measurements of $u^\star_{(h,\sigma_{\mathrm{output}})}$ at $\partial\Omega_h$, which are the Neumann data for the Helmholtz problem to be solved in Step 4.

In Figures 5(a)–(c) we depict the error $\mathrm{sd}_N|x^{(h,\sigma)} - x^\star|$ in the presence of $\sigma = \sigma_{\mathrm{input}}$, $\sigma = \sigma_{\mathrm{output}}$, and both $\sigma = (\sigma_{\mathrm{input}}, \sigma_{\mathrm{output}})$ simultaneously, in the range of 1–50% for various mesh sizes $h = \{2^{-6}, 2^{-5}, 2^{-4}, 2^{-3}, 2^{-2}\}$. From these plots we conclude that the error is of order $\mathrm{O}(h) + \mathrm{O}(\sigma)$. This can be explained by the linear dependence of the right-hand side on σ and by the $\mathrm{O}(h)$ approximation order of the Helmholtz equation. We note that growth of the error is rather low. Indeed, while we also depicted the result for coarse meshes, for reasonably fine meshes the error is much less than 1%. This result is very accurate in comparison with other methods known to us from the literature on identification problems.

Now we consider the error $|x^h - x^\star|$ due to discretization with mesh size h in the absence of noise. As we noted before, the error is zero when $x^\star$ coincides with mesh nodes, independently of h. Otherwise, the error has order $\mathrm{O}(h^4)$ as depicted in Figure 6(a) with the solid line. For comparison, we depict in plots (b) and (c) with the solid lines the respective errors $\mathrm{sd}_N|x^{(h,\sigma)} - x^\star|$ in the presence of input and output noises. In comparison with the latter ones, the discretization error is four(!) orders less, and hence negligible.

We note that the discretization error is rather sensitive to solvers which are applied to the underlying Helmholtz problem. Thus, we compared our solver based on the PGE with the standard GLS method, whose result is depicted in Figure 6 with the dashed lines. We report that the discretization error of GLS is four orders higher than PGE and comparable with the error due to noise. In the plots (b) and (c) we observe a moderate advantage of PGE over GLS with respect to noisy data, which is viewable for large noise levels σ.

The presented results allow us to declare the high precision and stability properties of the optimality-condition-based algorithm for identification of the object center in $\mathbb{R}^d$ from the intersection of d images.
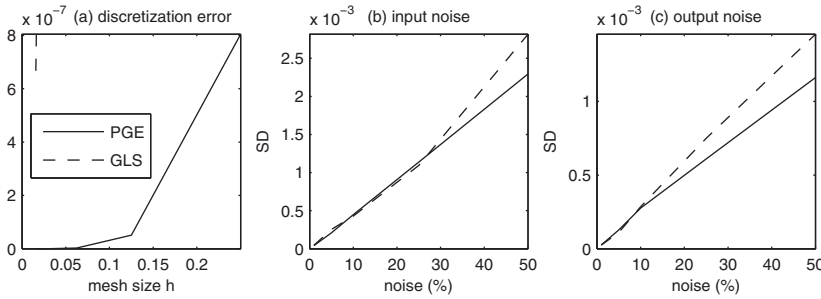
FIG. 6. *Comparison between errors due to discretization and noise for PGE and GLS solvers.*

4. Conclusion. We introduced a level set concept of imaging from multiple measurements for the inverse problem of identification of objects described in the abstract form. The concept has a broad scope. We specified our approach for the inverse Helmholtz problem identifying the center of a test object of arbitrary shape and unknown boundary conditions from a boundary measurement with the help of the imaging function deduced from optimality conditions. We justified that the respective identification algorithm obeys the high precision and stability properties with respect to discretization and noise. Further applications of our approach to more unknown geometric and physical variables to be identified are under development.

Appendix A. The asymptotic expansion in 2 dimensions. Here we justify rigorously the asymptotic expansion (3.15) of the objective function J which is defined in (3.14) for the case $d = 2$. For this purpose we construct asymptotic expansions of the Helmholtz problems (3.4), (3.12), and (3.13). The estimation needs the following uniform infsup condition: There exists $\beta_0 \in \mathbb{R}^+$ such that

$$(A.1) \qquad 0 < \beta_0 \le \inf_u \sup_v \frac{\left| \int_{\Omega \setminus \omega_\varepsilon(x_0)} (\nabla u \cdot \nabla \overline{v} - k^2 u \overline{v})\, dx + \int_{\partial \omega_\varepsilon(x_0)} \alpha u \overline{v}\, dS_x \right|}{\|u\|_{H^1(\Omega \setminus \overline{\omega_\varepsilon(x_0)}; \mathbb{C})} \|v\|_{H^1(\Omega \setminus \overline{\omega_\varepsilon(x_0)}; \mathbb{C})}}$$

for all $u, v \in H^1(\Omega \setminus \overline{\omega_\varepsilon(x_0)}; \mathbb{C})$, fixed $k \in \mathbb{R}$, and $(\omega, \varepsilon, x_0, \alpha) \in \widetilde{\Theta}$. By (A.1) existence of a unique solution to (3.4) follows.

We start with a local asymptotic representation of the background solutions u^0 and v^0 of (3.12) and (3.13). A local coordinate system associated with a trial center $x_0 \in \Omega \subset \mathbb{R}^2$ with the polar coordinates $\rho := |x - x_0|$ and $\theta \in (-\pi, \pi]$ for $x \in B_R(x_0)$ with such $R > 0$ that $B_R(x_0) \subset \Omega$ is introduced. Here $B_R(x_0)$ denotes a ball of radius R and center x_0. Using Bessel functions of the first kind $J_n(t)$, $n = 0, 1, \ldots$, we prove the following Fourier series.

LEMMA A.1. *The background solution $u^0 \in H^1(\Omega; \mathbb{C})$ of (3.12) admits the near field representation*

$$(A.2) \qquad u^0(x) = u^0(x_0) J_0(k\rho) + U^0(\rho, \theta) \quad in\ B_R(x_0) \subset \Omega$$

with the residual $U^0 \in H^1(B_R(x_0); \mathbb{C})$ such that

$$(A.3) \qquad \int_{-\pi}^{\pi} U^0\, d\theta = 0,$$

where

$$(A.4) \qquad U^0(\,\cdot\,, \theta) = O(k\rho) \quad for\ \rho \in [0, R],\ \theta \in (-\pi, \pi].$$

Proof. In the ball $B_\delta(x_0)$ with $\delta \in [0, R]$ we define the radial function $u_0^0(\rho) := \frac{1}{2\pi} \int_{-\pi}^{\pi} u^0(\rho, \theta)\, d\theta$ for $\rho \in (0, \delta)$, and set $U^0 := u^0 - u_0^0$. Therefore, the residual satisfies $U^0 \in H^1(B_R(x_0); \mathbb{C})$ and it fulfills (A.3). The substitution of a smooth cutoff function $\eta(\rho)$ supported in $B_\delta(x_0)$ as the test function $v = \eta$ into (3.12) leads to the relation

$$0 = \int_{B_\delta(x_0)} (\nabla u^0 \cdot \nabla \overline{\eta} - k^2 u^0 \overline{\eta})\, dx = -2\pi \int_0^\delta \Big(\big(\rho (u_0^0)'_\rho\big)'_\rho + k^2 \rho u_0^0 \Big) \overline{\eta}\, d\rho \quad \text{for all } \eta,$$

which results in the Bessel equation $(u_0^0)''_\rho + \frac{1}{\rho}(u_0^0)'_\rho + k^2 u_0^0 = 0$. Its general solution has the form $u_0^0(\rho) = K_0^0 J_0(k\rho) + S_0^0 Y_0(k\rho)$, $K_0^0, S_0^0 \in \mathbb{C}$, with the Neumann function $Y_0(t)$. But $Y_0(t) = \frac{2}{\pi} \ln \frac{t}{2} + \mathrm{O}(1)$ contradicts the fact $u_0^0 \in H^1(B_R(x_0); \mathbb{C})$, hence $S_0^0 = 0$ and $u_0^0(\rho) = K_0^0 J_0(k\rho)$. By continuing the expansion of the residual in the Fourier series $U^0 = \sum_{n=1}^{\infty} J_n(k\rho)((K_n^0)_1 \cos n\theta + (K_n^0)_2 \sin n\theta)$ with coefficients $K_n^0 \in \mathbb{C}^2$, we derive (A.4). Passing $\rho \searrow +0$ in the representation $u^0(x) = K_0^0 J_0(k\rho) + U^0(x)$ and due to the asymptotic property $J_0(t) = 1 + \mathrm{O}(t^2)$ and (A.4), we obtain $K_0^0 = u^0(x_0)$, and hence (A.2). This completes the proof. □

An assertion similar to Lemma A.1 holds for v^0.

LEMMA A.2. *The adjoint background solution $v^0 \in H^1(\Omega; \mathbb{C})$ of (3.13) admits the near field representation*

$$(\text{A.5}) \qquad\qquad v^0(x) = v^0(x_0) J_0(k\rho) + V^0(\rho, \theta) \quad \text{in } B_R(x_0) \subset \Omega,$$

with the residual $V^0 \in H^1(B_R(x_0); \mathbb{C})$ such that

$$(\text{A.6}) \qquad\qquad\qquad \int_{-\pi}^{\pi} V^0\, d\theta = 0,$$

where

$$(\text{A.7}) \qquad\qquad V^0(\,\cdot\,, \theta) = \mathrm{O}(k\rho) \quad \text{for } \rho \in [0, R],\ \theta \in (-\pi, \pi].$$

Next we expand the solution $u^{(\omega, \varepsilon, x_0, \alpha)}$ of the Helmholtz problem (3.4) as $\varepsilon \searrow +0$. This needs an auxiliary Laplace problem stated in the exterior domain $\mathbb{R}^2 \setminus \overline{\omega}$ with respect to the stretched variable $y = \frac{x - x_0}{\varepsilon}$. For this reason we introduce the weighted Sobolev spaces

$$W_\mu^{1,p}(\mathbb{R}^2 \setminus \overline{\omega}; \mathbb{C}) = \{v :\ \tfrac{v}{\mu}, \nabla v \in L^p(\mathbb{R}^2 \setminus \overline{\omega}; \mathbb{C})\}, \quad p \in (1, \infty),$$

with the weight $\mu(y) \sim |y| \ln |y|$ in $\mathbb{R}^2 \setminus \overline{B_1(0)}$ suggested by the weighted Poincaré inequality in exterior domains; see [15]. In these spaces we state the following auxiliary result.

LEMMA A.3. *For given $\alpha(y) \in L^\infty(\partial\omega; \mathbb{C})$ and arbitrary $p > 2$, $\frac{1}{p} + \frac{1}{p'} = 1$, there exists the variational solution of the following exterior Neumann problem: Find $w^\alpha(y) \in W_\mu^{1,p}(\mathbb{R}^2 \setminus \overline{\omega}; \mathbb{C})$ such that*

$$(\text{A.8}) \qquad \int_{\mathbb{R}^2 \setminus \omega} \nabla w^\alpha \cdot \nabla \overline{v}\, dy = \int_{\partial\omega} \alpha \overline{v}\, dS_y \quad \text{for all } v \in W_\mu^{1,p'}(\mathbb{R}^2 \setminus \overline{\omega}; \mathbb{C}),$$

which admits, after rescaling $y = \frac{x - x_0}{\varepsilon}$, the far field representation in the Fourier series as

$$(\text{A.9}) \qquad w^\alpha\big(\tfrac{x - x_0}{\varepsilon}\big) = -\langle \alpha \rangle \ln \rho + W^\alpha(\rho, \theta) \quad \text{for all } x \in \mathbb{R}^2 \setminus \overline{B_\varepsilon(x_0)}$$

with $\langle \alpha \rangle := \frac{1}{2\pi} \int_{\partial \omega} \alpha(y) \, dS_y$ *and the residual* $W^\alpha(x) \in W_\mu^{1,2}(\mathbb{R}^2 \setminus \overline{B_\varepsilon(x_0)}; \mathbb{C})$ *such that*

$$(A.10) \qquad \int_{-\pi}^{\pi} W^\alpha \, d\theta = 0, \quad W^\alpha(\cdot, \theta) = \mathrm{O}(\|\alpha\|_\infty \tfrac{\varepsilon}{\rho}) \quad \text{for } \rho > \varepsilon, \ \theta \in (-\pi, \pi].$$

Proof. The existence of a solution to (A.8) up to a free constant $c \in \mathbb{C}$ follows from the results of [15].

We take $R \geq 1$ such that $\omega \subset B_1(0) \subset B_R(0)$ and split further $\mathbb{R}^2 \setminus \overline{\omega}$ in the near field $B_R(0) \setminus \overline{\omega}$ and the far field $\mathbb{R}^2 \setminus \overline{B_R(0)}$. In $B_R(0) \setminus \overline{\omega}$, a Green formula can be used, which leads to the following relation

$$(A.11) \qquad \int_{B_R(0)\setminus\omega} \nabla w^\alpha \cdot \nabla \overline{v} \, dy = \int_{\partial \omega} \alpha \overline{v} \, dS_y + \int_{\partial B_R(0)} \frac{\partial w^\alpha}{\partial n} \overline{v} \, dS_y,$$

which holds for all $v \in H^1(B_R(0) \setminus \overline{\omega}; \mathbb{C})$ due to $\Delta w^\alpha = 0$ in $B_R(0) \setminus \overline{\omega}$ and $\frac{\partial w^\alpha}{\partial n} = \alpha$ at $\partial \omega$. In $\mathbb{R}^2 \setminus \overline{B_R(0)}$, we can apply the Fourier series to the harmonic function w^α as

$$(A.12) \qquad w^\alpha(y) = c + c_0^\alpha \ln |y| + \sum_{n=1}^{\infty} |y|^{-n} ((c_n^\alpha)_1 \cos n\theta + (c_n^\alpha)_2 \sin n\theta)$$

with unknown coefficients $c_0^\alpha \in \mathbb{C}$, $c_n^\alpha \in \mathbb{C}^2$, $n = 1, 2, \ldots$. Substituting (A.12) as $|y| = R$ into (A.11) and plugging in the test function $v \equiv 1$, it follows that $0 = \int_{\partial \omega} \alpha(y) \, dS_y + 2\pi c_0^\alpha$. Hence we find $c_0^\alpha = -\langle \alpha \rangle$. We take the free constant $c = c_0^\alpha \ln \varepsilon$ so that, after rescaling $y = \frac{x - x_0}{\varepsilon}$, the decomposition (A.12) implies (A.9) and follows the properties (A.10). The estimation $\mathrm{O}(\|\alpha\|_\infty)$ here is due to the linearity of problem (A.8) in α. The proof is completed. $\square$

With the help of Lemma A.1 and Lemma A.3 we expand the perturbed solution $u^{(\omega, \varepsilon, x_0, \alpha)}$ in small ε.

LEMMA A.4. *The solution* $u^{(\omega, \varepsilon, x_0, \alpha)} \in H^1(\Omega \setminus \overline{\omega_\varepsilon(x_0)}; \mathbb{C})$ *of* (3.4) *admits the representation*

$$(A.13) \qquad u^{(\omega, \varepsilon, x_0, \alpha)}(x) = u^0(x) - \varepsilon u^0(x_0) w^\alpha\left(\tfrac{x - x_0}{\varepsilon}\right) + Q(x) \quad \text{for } x \in \Omega \setminus \overline{\omega_\varepsilon(x_0)},$$

with the residual term $Q \in H^1(\Omega \setminus \overline{\omega_\varepsilon(x_0)}; \mathbb{C})$ *satisfying*

$$(A.14) \qquad \|Q\|_{H^1(\Omega\setminus\overline{\omega_\varepsilon(x_0)};\mathbb{C})} = \mathrm{O}\big((1 + \|\alpha\|_\infty + \|\alpha\|_\infty^2 \varepsilon)\varepsilon\big).$$

Proof. Applying Green's formula in $\Omega \setminus \omega_\varepsilon(x_0)$ we derive from (3.12)

$$(A.15) \qquad \begin{aligned} &\int_{\Omega\setminus\omega_\varepsilon(x_0)} (\nabla u^0 \cdot \nabla \overline{v} - k^2 u^0 \overline{v}) \, dx + \int_{\partial \omega_\varepsilon(x_0)} \alpha u^0 \overline{v} \, dS_x \\ &= \int_{\partial \Omega} g \overline{v} \, dS_x + \int_{\partial \omega_\varepsilon(x_0)} \left(\frac{\partial u^0}{\partial n} + \alpha u^0 \right) \overline{v} \, dS_x. \end{aligned}$$

Again by the Green formula we compute from (A.8)

$$(A.16) \qquad \begin{aligned} &\int_{\Omega\setminus\omega_\varepsilon(x_0)} (\nabla w^\alpha \cdot \nabla \overline{v} - k^2 w^\alpha \overline{v}) \, dx + \int_{\partial \omega_\varepsilon(x_0)} \alpha w^\alpha \overline{v} \, dS_x \\ &= \int_{\partial \Omega} \frac{\partial w^\alpha}{\partial n} \overline{v} \, dS_x - k^2 \int_{\Omega\setminus\omega_\varepsilon(x_0)} w^\alpha \overline{v} \, dx + \int_{\partial \omega_\varepsilon(x_0)} \alpha(w^\alpha + \tfrac{1}{\varepsilon}) \overline{v} \, dS_x. \end{aligned}$$

Subtracting (A.15) from (3.4) and adding (A.16) multiplied by $\varepsilon u^0(x_0)$, we obtain the following equation for the residual $Q := u^{(\omega,\varepsilon,x_0,\alpha)} - u^0 + \varepsilon u^0(x_0)w^\alpha$ and for all $v \in H^1(\Omega \setminus \overline{\omega_\varepsilon(x_0)}; \mathbb{C})$:

$$(A.17) \qquad \int_{\Omega \setminus \omega_\varepsilon(x_0)} (\nabla Q \cdot \nabla \overline{v} - k^2 Q \overline{v})\, dx + \int_{\partial \omega_\varepsilon(x_0)} \alpha Q \overline{v}\, dS_x = F(v),$$

with the linear right-hand side

$$F(v) := \varepsilon u^0(x_0) \int_{\partial\Omega} \frac{\partial w^\alpha}{\partial n} \overline{v}\, dS_x - \varepsilon u^0(x_0) k^2 \int_{\Omega \setminus \omega_\varepsilon(x_0)} w^\alpha \overline{v}\, dx$$
$$+ \int_{\partial \omega_\varepsilon(x_0)} \Big(\alpha(u^0(x_0) - u^0) - \frac{\partial u^0}{\partial n} + \varepsilon u^0(x_0) \alpha w^\alpha \Big) \overline{v}\, dS_x.$$

To evaluate $F(v)$, in the far field $\Omega \setminus \overline{B_\varepsilon(x_0)}$ we use (A.9) and (A.10). In the near field $B_\varepsilon(x_0) \setminus \overline{\omega_\varepsilon(x_0)}$ we apply (A.2), (A.4), and homogeneity arguments yielding

$$\|u\|_{L^2(B_\varepsilon(x_0) \setminus \overline{\omega_\varepsilon(x_0)}; \mathbb{C})} \le c_1 \varepsilon \|\nabla u\|_{L^2(B_\varepsilon(x_0) \setminus \overline{\omega_\varepsilon(x_0)}; \mathbb{C})},$$
$$\|u\|_{L^2(\partial\omega_\varepsilon(x_0); \mathbb{C})} \le c_2 \sqrt{\varepsilon} \|\nabla u\|_{L^2(B_\varepsilon(x_0) \setminus \overline{\omega_\varepsilon(x_0)}; \mathbb{C})} \text{ for } u \in H^1(B_\varepsilon(x_0) \setminus \overline{\omega_\varepsilon(x_0)}; \mathbb{C}).$$

Since $\|\nabla w^\alpha\|_{L^2(\Omega \setminus \overline{\omega_\varepsilon(x_0)}; \mathbb{C})} = \mathrm{O}(\|\alpha\|_\infty)$ these inequalities imply the following estimates:

$$\|\alpha(u^0(x_0) - u^0) - \tfrac{\partial u^0}{\partial n}\|_{C(\partial\omega_\varepsilon(x_0); \mathbb{C})} = \mathrm{O}(\|\alpha\|_\infty \varepsilon + 1), \quad \|\tfrac{\partial w^\alpha}{\partial n}\|_{C(\partial\Omega; \mathbb{C})} = \mathrm{O}(\|\alpha\|_\infty),$$
$$\|w^\alpha\|_{L^2(\Omega \setminus \overline{\omega_\varepsilon(x_0)}; \mathbb{C})} = \mathrm{O}\big(\|\alpha\|_\infty (1 + \varepsilon)\big),$$
$$\|w^\alpha\|_{L^2(\partial\omega_\varepsilon(x_0); \mathbb{C})} = \mathrm{O}(\|\alpha\|_\infty \sqrt{\varepsilon}).$$

Applying the Cauchy–Schwarz inequality to the expression defining F we arrive at $|F(v)| \le c_3((1 + \|\alpha\|_\infty + \|\alpha\|_\infty^2 \varepsilon)\varepsilon)\|v\|_{H^1(\Omega \setminus \overline{\omega_\varepsilon(x_0)}; \mathbb{C})}$. With the help of the infsup condition (A.1), and from (A.17) we infer (A.14). The proof is completed. $\quad\square$

From Lemmas A.1–A.4 we finish with the main result of this section.

THEOREM A.5. *The objective function J from* (3.14) *admits the asymptotic representation* (3.15) *due to the following expansion in small $\varepsilon \searrow +0$:*

$$(A.18) \qquad -\mathrm{Re}\left\{ \int_{\partial\Omega} (u^{(\omega,\varepsilon,x_0,\alpha)} - u^0)\tfrac{\partial \overline{v}^0}{\partial n}\, dS_x \right\} = 2\pi\varepsilon\, \mathrm{Re}\{\langle\alpha\rangle u^0(x_0)\overline{v^0}(x_0)\}$$
$$+ \mathrm{O}\big((1 + \|\alpha\|_\infty + \|\alpha\|_\infty^2 \varepsilon)^2 \varepsilon^2\big).$$

Proof. Indeed, from (A.13) and (A.14) it follows that

$$\int_{\partial\Omega} |u^{(\omega,\varepsilon,x_0,\alpha)} - u^0|^2\, dS_x = \mathrm{O}\big((1 + \|\alpha\|_\infty |\ln\varepsilon| + \|\alpha\|_\infty^2 \varepsilon)^2 \varepsilon^2\big).$$

Thus, once (A.18) was proved, then (3.15) follows from (3.14).

To prove (A.18) we apply the second Green formula in $\Omega \setminus \overline{B_\varepsilon(x_0)}$ and rewrite the integral over $\partial\Omega$ on the left-hand side of (A.18) equivalently over the circle $\partial B_\varepsilon(x_0)$

$$(A.19)$$
$$-\int_{\partial\Omega} (u^{(\omega,\varepsilon,x_0,\alpha)} - u^0)\tfrac{\partial \overline{v}^0}{\partial n}\, dS_x = \mathcal{I}_1 + \mathcal{I}_2,$$

$$\mathcal{I}_1 := \int_{\partial B_\varepsilon(x_0)} (u^{(\omega,\varepsilon,x_0,\alpha)} - u^0)\tfrac{\partial \overline{v}^0}{\partial n}\, dS_x, \quad \mathcal{I}_2 := -\int_{\partial B_\varepsilon(x_0)} \tfrac{\partial(u^{(\omega,\varepsilon,x_0,\alpha)} - u^0)}{\partial n} \overline{v}^0\, dS_x.$$

Now we can calculate analytically $\mathcal{I}_1$ and $\mathcal{I}_2$ on the right-hand side of (A.19) by substituting here the asymptotic representations (A.2), (A.5), (A.9), and (A.13). We apply homogeneity arguments and conclude from the trace theorem that

$$\|u\|_{L^2(\partial B_\varepsilon(x_0);\mathbb{C})} \leq c_4 \sqrt{\varepsilon} \|\nabla u\|_{L^2(B_R(x_0)\setminus\overline{B_\varepsilon(x_0)};\mathbb{C})} \quad \text{for } u \in H^1(B_R(x_0)\setminus\overline{B_\varepsilon(x_0)};\mathbb{C}).$$

With this inequality we derive

$$\mathcal{I}_1 = \int_{\partial B_\varepsilon(x_0)} (\varepsilon u^0(x_0)w^\alpha + Q)(\overline{v^0}(x_0)\tfrac{\partial J_0}{\partial n} + \tfrac{\partial \overline{V^0}}{\partial n})\, dS_x$$

$$= \varepsilon u^0(x_0) \int_{-\pi}^{\pi} w^\alpha(\varepsilon,\theta)\big(\overline{v^0}(x_0)kJ_1(k\varepsilon) - \tfrac{\partial \overline{V^0}}{\partial \rho}(\varepsilon,\theta)\big)\varepsilon d\theta - \int_{\partial B_\varepsilon(x_0)} Q\tfrac{\partial \overline{v^0}}{\partial \rho}\, dS_x$$

and estimate its absolute value using (A.6), (A.7), and (A.10):

$$(A.20) \quad \begin{aligned} |\mathcal{I}_1| &\leq c_5\|\alpha\|_\infty \varepsilon^2 + c_6\sqrt{\varepsilon}\|Q\|_{H^1(B_R(x_0)\setminus\overline{B_\varepsilon(x_0)};\mathbb{C})} \times \sqrt{\varepsilon}\|\tfrac{\partial v^0}{\partial \rho}\|_{H^1(B_R(x_0)\setminus\overline{B_\varepsilon(x_0)};\mathbb{C})} \\ &= \mathrm{O}\big((1 + \|\alpha\|_\infty + \|\alpha\|_\infty^2 \varepsilon)\varepsilon^2\big). \end{aligned}$$

For the calculation of $\mathcal{I}_2$ in (A.19), the zero mean property of W^α from (A.10) is useful. With its help we infer that

$$\mathcal{I}_2 = \int_{\partial B_\varepsilon(x_0)} \big(u^0(x_0)(\langle\alpha\rangle - \varepsilon\tfrac{\partial W^\alpha}{\partial n}) - \tfrac{\partial Q}{\partial n}\big)(\overline{v^0}(x_0)J_0 + \overline{V^0})\, dS_x$$

$$= u^0(x_0)\langle\alpha\rangle \int_{-\pi}^{\pi} (\overline{v^0}(x_0)J_0(k\varepsilon) + \overline{V^0}(\varepsilon,\theta))\varepsilon d\theta + \varepsilon u^0(x_0)\int_{-\pi}^{\pi} \tfrac{\partial W^\alpha}{\partial \rho}\overline{V^0}\varepsilon d\theta$$

$$- \int_{\partial B_\varepsilon(x_0)} \tfrac{\partial Q}{\partial n}\overline{v^0}\, dS_x = 2\pi\varepsilon\,\langle\alpha\rangle u^0(x_0)\overline{v^0}(x_0) + \mathrm{O}(\|\alpha\|_\infty\varepsilon^2) - \int_{\partial B_\varepsilon(x_0)} \tfrac{\partial Q}{\partial n}\overline{v^0}\, dS_x.$$

Next applying the Green formula in $B_\varepsilon(x_0)\setminus\overline{\omega_\varepsilon(x_0)}$ we have from (A.17)

$$-\int_{\partial B_\varepsilon(x_0)} \tfrac{\partial Q}{\partial n}\overline{v^0}\, dS_x = -\int_{B_\varepsilon(x_0)\setminus\omega_\varepsilon(x_0)} (\nabla Q \cdot \nabla\overline{v^0} - k^2 Q\overline{v^0})\, dx$$

$$+ \int_{\partial\omega_\varepsilon(x_0)} \big(-\alpha Q + \alpha(u^0(x_0) - u^0) + \varepsilon u^0(x_0)\alpha w^\alpha - \tfrac{\partial u^0}{\partial n}\big)\overline{v^0}\, dS_x.$$

Estimating its terms and using the representation

$$-\int_{\partial\omega_\varepsilon(x_0)} \tfrac{\partial u^0}{\partial n}\overline{v^0}\, dS_x$$

$$= \int_{\partial\omega_\varepsilon(x_0)} (u^0(x_0)kJ_1\tfrac{x\cdot n}{\rho} - \nabla u^0(x_0)\cdot n - \tfrac{\partial U^1}{\partial n}) \times (\overline{v^0}(x_0)J_0 + \overline{V^0})\, dS_x = \mathrm{O}(\varepsilon^2)$$

with the residual term $U^1 = \mathrm{O}((k\rho)^2)$ in the second order asymptotic expansion $u^0(x) = u^0(x_0)J_0(k\rho) + 2J_1(k\rho)\nabla u^0(x_0)\cdot\tfrac{x}{\rho} + U^1(x)$ (compare with (A.2)), we derive

$$\left|\int_{\partial B_\varepsilon(x_0)} \tfrac{\partial Q}{\partial n}\overline{v^0}\, dS_x\right| \leq c_7(1 + \|\alpha\|_\infty)\big(1 + \|\alpha\|_\infty + \|\alpha\|_\infty^2 \varepsilon\big)\varepsilon^2.$$

Therefore, the following relation holds

$$(A.21) \qquad \mathcal{I}_2 = 2\pi\varepsilon \langle\alpha\rangle u^0(x_0)\overline{v^0}(x_0) + \mathrm{O}\big((1 + \|\alpha\|_\infty + \|\alpha\|_\infty^2 \varepsilon)^2 \varepsilon^2\big).$$

From (A.19),(A.20), and (A.21) we infer (A.18) and the assertion of the theorem. □

Finally, we note that $\mathcal{I}_1$ and $\mathcal{I}_2$ in (A.19) can be rewritten over arbitrary closed contours in $\Omega \setminus \overline{\omega_\varepsilon(x_0)}$ thus implying the invariant integral.

REFERENCES

[1] G. ALESSANDRINI AND L. RONDI, *Determining a sound-soft polyhedral scatterer by a single far-field measurement*, Proc. Amer. Math. Soc., 133 (2005), pp. 1685–1691.

[2] G. ALLAIRE, F. DE GOURNAY, F. JOUVE, AND A.-M. TOADER, *Structural optimization using topological and shape sensitivity via a level set method*, Control Cybernet., 34 (2005), pp. 59–80.

[3] L. AMBROSIO AND H.M. SONER, *Level set approach to mean curvature flow in arbitrary codimension*, J. Differential Geom., 43 (1996), pp. 693–737.

[4] H. AMMARI, E. BERETTA, E. FRANCINI, H. KANG, AND M. LIM, *Optimization algorithm for reconstructing interface changes of a conductivity inclusion from modal measurements*, Math. Comp., 79 (2010), pp. 1757–1777.

[5] H. AMMARI, E. BERETTA, E. FRANCINI, H. KANG, AND M. LIM, *Reconstruction of small interface changes of an inclusion from modal measurements* II: *The elastic case*, J. Math. Pures Appl. (9), 94 (2010), pp. 322–339.

[6] H. AMMARI, P. GARAPON, F. JOUVE, H. KANG, M. LIM, AND S. YU, *A new optimal control approach for the reconstruction of extended inclusions*, SIAM J. Control Optim., 51 (2013), pp. 1372–1394.

[7] H. AMMARI, J. GARNIER, V. JUGNON, AND H. KANG, *Stability and resolution analysis for a topological derivative based imaging functional*, SIAM J. Control Optim., 50 (2012), pp. 48–76.

[8] H. AMMARI, R. GRIESMAIER, AND M. HANKE, *Identification of small inhomogeneities: Asymptotic factorization*, Math. Comp., 76 (2007), pp. 1425–1448.

[9] H. AMMARI, J. GARNIER, H. KANG, W.-K. PARK, AND K. SØLNA, *Imaging schemes for perfectly conducting cracks*, SIAM J. Appl. Math., 71 (2011), pp. 68–91.

[10] H. AMMARI, J. GARNIER, AND K. SOLNA, *A statistical approach to target detection and localization in the presence of noise*, Waves Random Complex Media, 22 (2012), pp. 40–65.

[11] H. AMMARI AND H. KANG, *Reconstruction of Small Inhomogeneities From Boundary Measurements*, Springer-Verlag, Berlin, 2004.

[12] H. AMMARI, H. KANG, E. KIM, AND J.-Y. LEE, *The generalized polarization tensors for resolved imaging Part* II: *Shape and electromagnetic parameters reconstruction of an electromagnetic inclusion from multistatic measurements*, Math. Comp., 81 (2012), pp. 839–860.

[13] H. AMMARI, H. KANG, H. LEE, AND W.-K. PARK, *Asymptotic imaging of perfectly conducting cracks*, SIAM J. Sci. Comput., 32 (2010), pp. 894–922.

[14] H. AMMARI, H. KANG, M. LIM, AND H. ZRIBI, *The generalized polarization tensors for resolved imaging, Part* I: *Shape reconstruction of a conductivity inclusion*, Math. Comp., 81 (2012), pp. 367–386.

[15] C. AMROUCHE, V. GIRAULT, AND J. GIROIRE, *Dirichlet and Neumann exterior problems for the n-dimensional Laplace operator: An approach in weighted Sobolev spaces*, J. Math. Pures Appl. (9), 76 (1997), pp. 55–81.

[16] S. AMSTUTZ AND N. DOMINQUEZ, *Topological sensitivity analysis in the context of ultrasonic nondestructive testing*, Eng. Anal. Bound. Elem., 32 (2008), pp. 936–947.

[17] T. ARENS, D. GINTIDES, AND A. LECHLEITER, *Variational formulations for scattering in a three-dimensional acoustic waveguide*, Math. Methods Appl. Sci., 31 (2008), pp. 821–847.

[18] L. BEILINA AND C. CLASON, *An adaptive hybrid FEM/FDM method for an inverse scattering problem in scanning acoustic microscopy*, SIAM J. Sci. Comput., 28 (2006), pp. 382–402.

[19] M. BRÜHL, M. HANKE, AND M. VOGELIUS, *A direct impedance tomography algorithm for locating small inhomogeneities*, Numer. Math., 93 (2003), pp. 635–654.

[20] M. BURGER, B. HACKL, AND W. RING, *Incorporating topological derivatives into level set methods*, J. Comput. Phys., 194 (2004), pp. 344–362.

[21] F. CAKONI, D. COLTON, AND H. HADDAR, *The linear sampling method for anisotropic media*, J. Comput. Appl. Math., 146 (2002), pp. 285–299.

[22] A. CARPIO AND M.L. RAPÚN, *Topological derivatives for shape reconstruction*, in Inverse Problems and Imaging, Lecture Notes in Math. 1943, Springer, Berlin, 2008, pp. 85–133.

[23] S. CHAABANE AND M. JAOUA, *Identification of Robin coefficients by the means of boundary measurements*, Inverse Problems, 15 (1999), pp. 1425–1438.

[24] S.N. CHANDLER-WILDE AND P. MONK, *Existence, uniqueness, and variational methods for scattering by unbounded rough surfaces*, SIAM J. Math. Anal., 37 (2005), pp. 598–618.

[25] D. COLTON AND F. CAKONI, *The determination of the surface impedance of a partially coated obstacle from far field data*, SIAM J. Appl. Math., 64 (2004), pp. 709–723.

[26] D. COLTON AND R. KRESS, *Inverse Acoustic and Electromagnetic Scattering Theory*, Springer-Verlag, Berlin, 1998.

[27] M. COSTABEL AND M. DAUGE, *A singularly perturbed mixed boundary value problem*, Comm. Partial Differential Equations, 21 (1996), pp. 1919–1949.

[28] A.J. DEVANEY, *Super-resolution processing of multi-static data using time reversal and MUSIC*, Technical report, Northeastern University, Boston, 2000.

[29] A. FRIEDMAN AND M. VOGELIUS, *Identification of small inhomogeneities of extreme conductivity by boundary measurements: A theorem on continuous dependence*, Arch. Ration. Mech. Anal., 105 (1989), pp. 299–326.

[30] J. GOMES AND O. FAUGERAS, *The vector distance functions*, Int. J. Comput. Vision, 52 (2003), pp. 161–187.

[31] R. GRIESMAIER, *Multi-frequency orthogonality sampling for inverse obstacle scattering problems*, Inverse Problems, 27 (2011), 085005.

[32] B.B. GUZINA AND M. BONNET, *Small-inclusion asymptotic of misfit functionals for inverse problems in acoustics*, Inverse Problems, 22 (2006), pp. 1761–1785.

[33] A. HERWIG, *Elliptische Randwertprobleme zweiter Ordnung in Gebieten mit einer Fehlstelle*, Z. Anal. Anwendungen, 8 (1989), pp. 153–161.

[34] M. HINTERMÜLLER AND V.A. KOVTUNENKO, *From shape variation to topology changes in constrained minimization: A velocity method-based concept*, Optim. Methods Softw., 26 (2011), pp. 513–532.

[35] M. IKEHATA AND H. ITOU, *On reconstruction of an unknown polygonal cavity in a linearized elasticity with one measurement*, J. Phys. Conf. Ser., 290 (2011), 012005.

[36] K. ITO, K. KUNISCH, AND Z. LI, *Level-set function approach to an inverse interface problem*, Inverse Problems, 17 (2001), pp. 1225–1242.

[37] B. KALTENBACHER, A. NEUBAUER, AND O. SCHERZER, *Iterative Regularization Methods for Nonlinear Ill-Posed Problems*, de Gruyter, Berlin, 2008.

[38] A.M. KHLUDNEV AND V.A. KOVTUNENKO, *Analysis of Cracks in Solids*, WIT-Press, Southampton, Boston, 2000.

[39] A.M. KHLUDNEV, V.A. KOVTUNENKO, AND A. TANI, *On the topological derivative due to kink of a crack with non-penetration. Anti-plane model*, J. Math. Pures Appl. (9), 94 (2010), pp. 571–596.

[40] A. KIRSCH, *An Introduction to the Mathematical Theory of Inverse Problems*, Springer, New York, 2011.

[41] R.V. KOHN AND M. VOGELIUS, *Relaxation of a variational method for impedance computed tomography*, Comm. Pure Appl. Math., 40 (1987), pp. 745–777.

[42] V.A. KOVTUNENKO, *State-constrained optimization for identification of small inclusions*, Proc. Appl. Math. Mech., 11 (2011), pp. 721–722.

[43] V.A. KOVTUNENKO AND K. KUNISCH, *Problem of crack perturbation based on level sets and velocities*, Z. Angew. Math. Mech., 87 (2007), pp. 809–830.

[44] V.A. KOVTUNENKO, K. KUNISCH, AND W. RING, *Propagation and bifurcation of cracks based on implicit surfaces and discontinuous velocities*, Comput. Vis. Sci., 12 (2009), pp. 397–408.

[45] A. LITMAN, D. LESSELIER, AND F. SANTOSA, *Reconstruction of a two-dimensional binary obstacle by controlled evolution of a level-set*, Inverse Problems, 14 (1998), pp. 685–706.

[46] H. LIU AND J. ZOU, *On unique determination of partially coated polyhedral scatterers with far field measurements*, Inverse Problems, 23 (2007), pp. 297–308.

[47] D.R. LUKE AND R. POTTHAST, *The no response test—a sampling method for inverse scattering problems*, SIAM J. Appl. Math., 63 (2003), pp. 1292–1312.

[48] V.G. MAZ'YA, S.A. NAZAROV, AND B.A. PLAMENEVSKI, *Asymptotic Theory of Elliptic Boundary Value Problems in Singularly Perturbed Domains*, Birkhäuser, Basel, 2000.

[49] S.A. NAZAROV AND J. SOKOLOWSKI, *Asymptotic analysis of shape functionals*, J. Math. Pures Appl. (9), 82 (2003), pp. 125–196.

[50] R. POTTHAST, J. SYLVESTER, AND S. KUSIAK, *A "range test" for determining scatterers with unknown physical properties*, Inverse Problems, 19 (2003), pp. 53–547.

[51] B. Samet, S. Amstutz, and M. Masmoudi, *The topological asymptotic for the Helmholtz equation*, SIAM J. Control Optim., 42 (2003), pp. 1523–1544.
[52] O. Scherzer, H.W. Engl, and K. Kunisch, *Optimal a posteriori parameter choice for Tikhonov regularization for solving nonlinear ill-posed problems*, SIAM J. Numer. Anal., 30 (1993), pp. 1796–1838.
[53] R.T. Smith, *An inverse acoustic scattering problem for an obstacle with an impedance boundary condition*, J. Math. Anal. Appl., 105 (1985), pp. 333–356.
[54] G.E. Stavroulakis, *Inverse and Crack Identification Problems in Engineering Mechanics*, Kluwer, Dordrecht, 2001.
[55] L.L. Thompson, *A review of finite element methods for time-harmonic acoustics*, J. Acoust. Soc. America, 119 (2006), pp. 1315–1330.